Rev. Mexicana Astron. Astrof., **24**, 155-177 (1992)

THE CHEMICAL COMPOSITION OF THE GALACTIC H II REGION M17

M. Peimbert[1,2], S. Torres-Peimbert[1,2]

Instituto de Astronomía
Universidad Nacional Autónoma de México

and

M.T. Ruiz[1]

Departamento de Astronomía
Universidad de Chile

Received 1992 June 3

RESUMEN

Presentamos espectrofotometría en el intervalo de 3400 a 7400 A de 17 áreas en M17. Las observaciones se obtuvieron en el Observatorio Nacional de Kitt Peak y en el Observatorio Interamericano de Cerro Tololo. Basados en estas observaciones determinamos la composición química de M17. Las abundancias por número expresadas logarítmicamente para $t^2 = 0.00$ son: H = 12.00, He = 11.02, C = 8.74, N = 7.71, O = 8.51, Ne = 7.80, S = 6.99, Cl = 5.18, Ar = 6.38, y Fe = 6.62; mientras que para $t^2 = 0.04$ son: H = 12.00, He = 11.00, C = 8.73, N = 8.01, O = 8.81, Ne = 8.13, S = 7.32, Cl = 5.48, Ar = 6.63, y Fe = 6.94.

Determinamos también por primera vez el gradiente galactocéntrico del cociente carbono a hidrógeno, d(C/H)/dR y es igual a -0.08 ± 0.02 dex kpc^{-1}. El cociente de helio a elementos pesados producidos en la galaxia $\Delta Y/\Delta Z$, derivado a partir de la abundancia primordial de helio y de las abundancias de M17, para $t^2 = 0.00$ es de 4.47 y para $t^2 = 0.04$ es de 2.50.

ABSTRACT

Spectrophotometry in the 3400-7400 A range is presented for 17 areas of the H II region M17. The observations were obtained at KPNO and CTIO with the 2.1-m and the 4-m telescopes respectively. Based on these observations the chemical composition is derived.

The logarithmic abundances by number of the gaseous component for $t^2 = 0.00$ are: H = 12.00, He = 11.02, C = 8.74, N = 7.71, O = 8.51, Ne = 7.80, S = 6.99, Cl = 5.18, Ar = 6.38, and Fe = 6.62; while for $t^2 = 0.04$ are: H = 12.00, He = 11.00, C = 8.73, N = 8.01, O = 8.81, Ne = 8.13, S = 7.32, Cl = 5.48, Ar = 6.63 and Fe = 6.94. The C abundance gradient in the Galaxy derived from the Orion nebula and M17 is of -0.08 ± 0.02 dex kpc^{-1}. The $\Delta Y/\Delta Z$ ratio derived from the primordial helium abundance and the M17 values amounts to 4.47 for $t^2 = 0.00$ and to 2.50 for $t^2 = 0.04$.

Key words: **NEBULAE-H II REGIONS – NEBULAE-ABUNDANCES**

I. INTRODUCTION

We decided to study M17 for the following reasons: a) It is a very bright H II region. b) It has a higher degree of ionization than the Orion nebula, therefore a smaller fraction of neutral helium is expected to be present inside M17 than in Orion, and consequently it should be possible to derive a

1. Visiting Astronomer, Cerro Tololo Interamerican Observatory operated by the Association of Universities for Research in Astronomy, Inc., under contract with the National Science Foundation.

2. Visiting Astronomer, KPNO, National Optical Astronomical Observatories, operated by the Association of Universities for Research in Astronomy, Inc., under contract with the National Science Foundation.

TABLE 1

POSITIONS, SIZES, FLUXES, EQUIVALENT WIDTHS, AND REDDENING CORRECTIONS FOR THE CTIO OBSERVATIONS

	Position[a]			log	EW(Hβ)	
Region	α	δ	size[b]	$F(H\beta)$	(A)	$C(H\beta)$
M17-1	140.5″W	250″S	42.5″	−12.27	562	1.90
M17-2	88.7 W	250 S	28.8	−12.35	617	1.85
M17-3	54.0 W	250 S	32.2	−11.88	708	1.72
M17-4	18.1 W	250 S	26.9	−12.33	589	1.85
M17-5	11.4 E	250 S	31.4	−12.11	646	1.60
M17-6	62.0 E	250 S	40.3	−12.09	603	1.25
M17-11	65.6 W	300 S	44.0	−12.15	603	1.50
M17-12	8.6 W	300 S	29.6	−12.15	631	1.50
M17-13	26.3 E	300 S	38.3	−11.75	832	1.45
M17-14	71.7 E	300 S	48.5	−11.70	776	1.20
M17-15	138.7 E	300 S	55.0	−11.81	741	1.10

[a] Relative to BD-16°4819; α (2000) = $18^h20^m43.6^s$, δ (2000) = −16°05′19″.
[b] Slit is 1.6″ wide.

more accurate He/H ratio. c) Through it, we can study the radial abundance gradient in the direction of the center of the Galaxy. d) Its heavy element abundance is higher than in the Orion nebula; therefore by comparing its chemical composition with the pregalactic helium abundance it is possible to derive a $\Delta Y/\Delta Z$ ratio of very high accuracy, this ratio can be used to test models of stellar evolution and galactic chemical evolution.

In §II we present the observations of eleven regions gathered at CTIO from long slit observations and of six regions gathered at KPNO, in §III we determine temperatures and densities; in §IV we compute the chemical abundances and in §V we compare the abundances of M17 with those of other objects and discuss the implications of our results.

II. OBSERVATIONS

a) *CTIO Spectroscopy*

Long slit spectra were obtained during two observing runs, in August and September 1990, with the 4-m telescope equipped with the R-C Spectrograph and a coated GEC CCD detector. Using three different gratings (at first order) the spectral ranges between λλ3440-5110, 4220-7360 and 5800-7370 were covered. The slit, oriented E-W, was 4.7 arcmin long and 1.6 arcsec wide; the scale along the dispersion axis was 0.73″/pixel. The resolution was 7 A for the blue and red wavelength ranges and 14 A for the intermediate one. The slit was placed at two different positions of the nebula, in these positions eleven extraction windows were defined avoiding bright stars that could contaminate the spectra. Table 1 gives a summary of the extraction windows, in Figure 1 the two positions of the slit are indicated on a reproduction of M17. A map with the stellar positions in M17 has been presented by Ogura & Ishida (1976); similarly radio maps indicating the positions of the ionizing stars have been presented by Felli, Churchwell, & Massi (1984).

To flux calibrate the spectra five or six spectrophotometric standards, from Stone & Baldwin (1983), were observed each night with the slit widened to 6.4″. A He-Ne-Ar lamp was used to perform the wavelength calibration. Dome-flats and sky-flats were obtained to flatten the red frames while a quartz lamp flat and a sky flat were used for the blue range frames. Several bias frames were taken each night. Data reduction was performed using the IRAF reduction package. To achieve a good sky subtraction a section of the long slit where there is no or little contribution from the nebula was chosen. Short exposure frames at each position were used to remove cosmic rays and to measure fluxes of strong lines saturated in the longer exposures. In Figures 2-4 we show typical spectra of single regions at one observing season.

In Table 2 we present the intrinsic line intensities, $I(\lambda)$, given by

$$log\left[\frac{I(\lambda)}{I(H\beta)}\right] = log\left[\frac{F(\lambda)}{F(H\beta)}\right] + C(H\beta)\,g(\lambda)\ ,$$

1992RMxAA..24..155P

LINE INTENSITIES FROM CTIO

λ	Id.	f(λ)	M17-1	M17-2	M17-3	M17-4	M17-5	M17-6	M17-11	M17-12	M17-13	M17-14	M17-15
3726+3729	[O II]	0.292	-0.01 2	+0.08 2	-0.16 2	-0.05 2	+0.16 2	+0.38 2	+0.16 2	-0.02 2	-0.15 2	+0.04 2	+0.37 2
3835	H9	0.261	-1.16 2	-1.14 2	-1.14 2	-1.16 3	-1.17 2	-1.13 2	-1.13 2	-1.16 2	-1.12 2	-1.12 2	-1.10 2
3869	[Ne III]	0.248	-0.61 2	-0.62 2	-0.64 2	-0.66 2	-0.74 2	-0.84 2	-0.78 2	-0.66 2	-0.66 2	-0.77 2	-0.89 2
3889	He I + H8	0.245	-0.75 2	-0.74 2	-0.82 3	-0.74 2	-0.76 2	-0.75 2	-0.68 2	-0.74 2	-0.79 2	-0.78 2	-0.74 2
3967+3970	[Ne III]+ H7	0.218	-0.67 2	-0.67 2	-0.66 2	-0.67 2	-0.69 2	-0.83 2	-0.67 2	-0.65 2	-0.64 2	-0.68 2	-0.71 2
4026	He I	0.208	-1.61 3	-1.61 3	-1.65 3	-1.63 3	-1.66 3	-1.66 3	-1.63 3	-1.69 4	-1.66 3	-1.63 3	-1.64 3
4068+4076	[S II]	0.194	-2.06 5	-2.01 5	-2.12 4	-2.04 5	-1.96 4	-1.76 4	-1.89 5	-1.95 5	-2.06 4	-1.98 4	-1.74 4
4102	Hδ	0.187	-0.59 1	-0.58 1	-0.59 1	-0.59 1	-0.59 1	-0.60 1	-0.59 1	-0.60 1	-0.59 1	-0.60 1	-0.59 1
4267	C II	0.144	-2.34 6	-2.27 6	-2.26 5	-2.23 6	-2.38 6	-2.38 6	-2.33 6	-2.37 6	-2.24 6	-2.35 5	...
4340	Hγ	0.125	-0.32 1	-0.32 1	-0.33 1	-0.32 1	-0.33 1	-0.33 1	-0.32 1	-0.33 1	-0.33 1	-0.33 1	-0.33 1
4363	[O III]	0.122	-1.90 4	-1.88 4	-1.95 3	-1.97 3	-1.96 3	-1.98 3	-1.99 4	-1.94 4	-2.00 4	-2.04 4	-2.10 4
4387	He I	0.119	...	-2.27 6	-2.26 5	-2.31 6	-2.30 6	-2.33 6	-2.29 5	-2.31 5	-2.22 5	-2.29 5	-2.32 5
4472	He I	0.097	-1.30 2	-1.29 2	-1.29 1	-1.29 2	-1.28 2	-1.31 2	-1.31 2	-1.30 2	-1.31 1	-1.32 1	-1.32 1
4641+4649	O II	0.047	-2.43 8	-2.41 8	-2.43 6	-2.38 8	-2.49 8	...	-2.42 8	-2.48 8	-2.53 8	-2.46 6	...
4658	[Fe III]	0.045	-2.28 6	-2.31 6	-2.38 6	-2.25 6	-2.30 6	-2.10 8	-2.28 6	-2.41 6	-2.39 6	-2.35 6	...
4713	He I + [Ar IV]	0.031	-2.19 3	-2.24 3	-2.20 3	-2.19 3	-2.24 4	-2.30 4	-2.27 4	-2.23 3	-2.23 3	-2.24 3	-2.32 3
4861	Hβ	0.000	0.00	0.00	0.00	0.00	0.00	0.00	0.00	0.00	0.00	0.00	0.00
4922+4930	He I + [O III]	-0.012	-1.86 3	-1.88 3	-1.83 3	-1.86 3	-1.86 3	-1.88 3	-1.86 3	-1.86 3	-1.87 3	-1.86 2	-1.86 3
4959	[O III]	-0.021	+0.16 1	+0.14 1	+0.12 1	+0.10 1	+0.07 1	+0.02 1	+0.03 1	+0.10 1	+0.09 1	+0.06 1	-0.02 1
5007	[O III]	-0.029	+0.64 1	+0.63 1	+0.61 1	+0.58 1	+0.54 1	+0.50 1	+0.51 1	+0.58 1	+0.57 1	+0.54 1	+0.45 1
5198+5200	[N I]	-0.080	-2.67 9	-2.81 9	-2.70 9	...	-2.53 9	-2.13 9	-2.52 9	-2.69 9	...	-2.42 9	-2.41 9
5518	[Cl III]	-0.146	-2.26 5	-2.33 5	-2.22 4	-2.28 5	-2.33 5	-2.25 5	-2.24 5	-2.27 5	-2.25 5	-2.29 5	-2.19 5
5538	[Cl III]	-0.151	-2.38 5	-2.39 5	-2.35 4	-2.36 5	-2.40 5	-2.27 5	-2.40 5	-2.41 5	-2.43 5	-2.46 5	-2.32 5
5755	[N II]	-0.198	-2.33 5	-2.31 5	-2.42 4	-2.56 5	-2.40 5	-2.07 4	-2.27 5	-2.36 5	-2.57 5	-2.52 5	-2.10 5
5876	He I	-0.218	-0.81 1	-0.81 1	-0.81 1	-0.82 1	-0.83 1	-0.84 1	-0.84 1	-0.83 1	-0.83 1	-0.83 1	-0.84 1
6311	[S III]	-0.305	-1.81 4	-1.81 4	-1.86 4	-1.90 4	-1.82 4	-1.75 4	...	-2.04 6	-1.93 6	-1.92 6	-1.82 5
6563	Hα	-0.348	+0.47 1	+0.48 1	+0.47 1	+0.48 1	+0.48 1	+0.47 1	+0.47 1	+0.46 1	+0.47 1	+0.47 1	+0.47 1
6583	[N II]	-0.354	-0.67 2	-0.62 2	-0.77 1	-0.74 2	-0.46 1	-0.14 1	-0.35 2	-0.55 2	-0.68 2	-0.66 1	-0.17 1
6678	He I	-0.374	-1.40 2	-1.42 1	-1.39 1	-1.41 2	-1.41 1	-1.41 1	-1.44 2	-1.44 2	-1.41 1	-1.41 1	-1.42 1
6716	[S II]	-0.384	-1.49 3	-1.42 3	-1.59 2	-1.55 3	-1.30 2	-0.95 2	-1.16 3	-1.41 3	-1.50 3	-1.34 2	-0.84 2
6731	[S II]	-0.386	-1.48 3	-1.39 3	-1.54 2	-1.50 3	-1.28 2	-0.96 2	-1.13 3	-1.37 3	-1.49 3	-1.34 2	-0.88 2
7065	He I	-0.416	-1.28 2	-1.31 2	-1.31 2	-1.34 2	-1.37 2	-1.43 2	-1.36 2	-1.40 2	-1.37 2	-1.43 2	-1.51 2
7136	[Ar III]	-0.428	-0.80 2	-0.80 2	-0.83 1	-0.85 2	-0.82 1	-0.80 1	-0.86 2	-0.85 2	-0.87 2	-0.86 2	-0.82 1
7231+7236	C II	-0.440	-2.40 6	-2.39 6	-2.34 5	-2.37 6	-2.43 6	-2.42 6	-2.43 6	-2.42 6	-2.33 6	-2.36 6	-2.45 6
7281	He I	-0.447	-2.23 5	-2.20 5	-2.15 4	-2.18 5	-2.22 4	-2.20 4	-2.25 5	-2.24 5	-2.20 5	-2.17 5	-2.20 5
7320+7330	[O II]	-0.452	-1.66 3	-1.60 3	-1.68 3	-1.72 3	-1.47 3	-1.29 3	-1.50 3	-1.60 3	-1.74 3	-1.67 3	-1.39 3

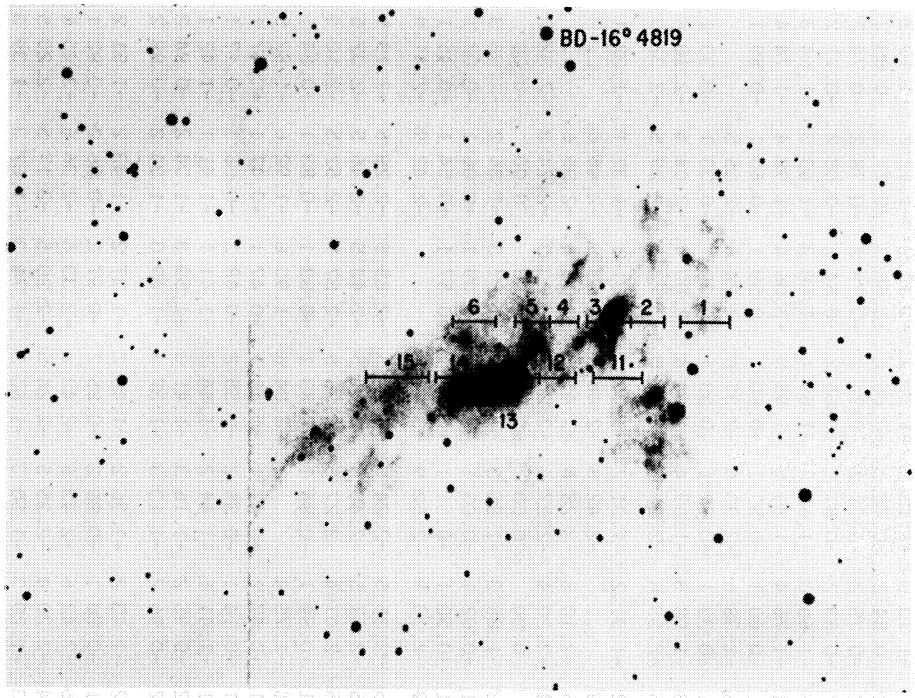

Fig. 1. Observed regions superposed to an Hα photograph of M17 (KPNO photograph), see Table 1.

where $F(\lambda)$ is the observed line flux corrected for atmospheric extinction and $C(H\beta)$ is the logarithmic reddening correction at Hβ, these quantities are presented in Table 1. The reddening function, $g(\lambda)$, is also presented in Table 1 and was obtained from the normal extinction law, $g'(\lambda)$ (Whitford 1958, as follows: $g(\lambda) = 1.04\ g'(\lambda)$ for $\lambda >$ Hβ and $g(\lambda) = g'(\lambda)/1.08$ for $\lambda <$ Hβ. $C(H\beta)$ and $g(\lambda)$ were obtained by fitting the observed Balmer decrement with that computed by Hummer & Storey (1987) for $N_e = 1000\ cm^{-3}$ and $T_e = 8000$ °K, the Balmer decrement is almost insensitive to N_e and T_e for the range of expected values. The differences between $g(\lambda)$ and $g'(\lambda)$ are small, they could be due to a systematic calibration error or more likely to a real difference in the reddening function; in both cases their effect on the determined line intensity ratios is negligible because after correction for reddening we recover the Balmer decrement, with a high degree of accuracy for regions with high and low $C(H\beta)$ values. To study further these differences a very accurate total absorption value is needed. The total absorption could be computed by comparing the Hβ flux with the radio flux, this comparison is beyond the scope of this paper.

In Table 2 the 1 σ error in the last digit is presented after each measurement, (i.e., the first intensity ratio is -0.01 ± 0.02), the errors were estimated by comparing the results derived from the two different seasons.

In Table 3 we present the line intensities of some O II recombination lines in M17-3 and M17-14 as well as upper limits for the $I(4686)/I(H\beta)$ ratios.

In Table 4 we present for M17-3 and M17-14 the equivalent widths in emission for the He I and H I lines, and in Table 5 the continuum observations for the same areas. By comparing the continuum observations with the expected atomic continua (e.g., Sánchez & Peimbert 1991) we find that for $\lambda = 4200$ A from 35% to 47% is due to atomic continua and the rest is due: a) to dust scattered light from the bright ionizing stars, and b) to a small contribution from faint stars projected into the slit. The atomic continuum is featureless, therefore to estimate the underlying H I and He I equivalent widths in absorption the EW of O stars should be multiplied by a factor of 0.6. From the absorption EW data in the literature for bright O stars we expect for Hβ and Hγ a maximum value of 2 A and for He I a maximum value of 0.4 A for $\lambda\lambda$4472, 5876 and 6678 (e.g., Conti 1971, 1973, 1974; Conti & Alschuler 1971; Auer & Mihalas 1972). By com-

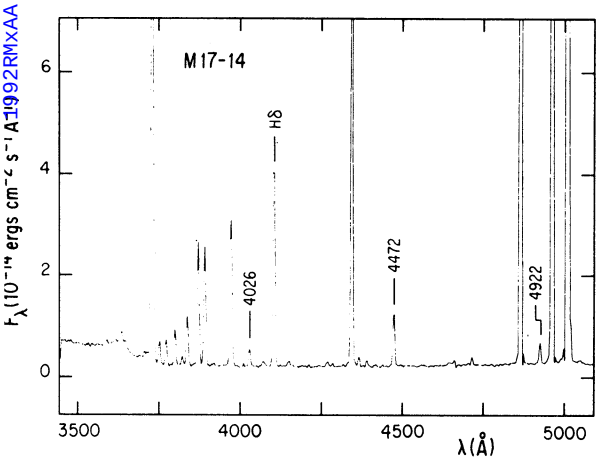

Fig. 2. Blue spectrogram of M17-14.

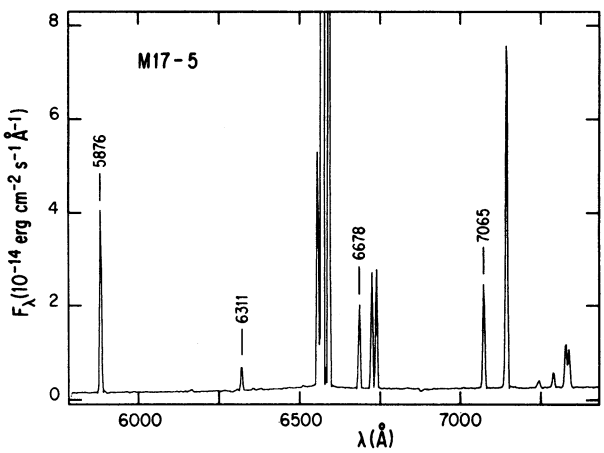

Fig. 4. Red spectrogram of M17-5.

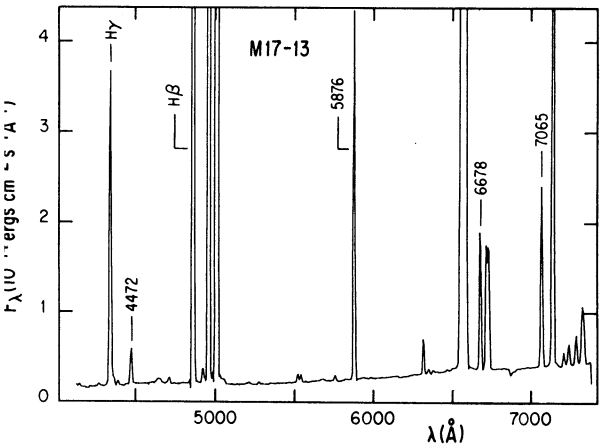

Fig. 3. Hα-Hβ spectrogram of M17-13.

paring the maximum expected EW in absorption with the observed EW in emission in Table 4 we find that the underlying absorption effect on the intensity of λ4472 is smaller than 1.3% and for the other lines is smaller than 1% . In what follows the underlying absorption effect on the emission line intensities will be neglected.

b) *KPNO Spectroscopy*

The observations were carried out with the 2.1-m telescope during May and September of 1978 with the Gold spectrograph and the intensified image dissector scanner (IDS). The IDS is a dual-beam multichannel spectrometer, each spectrum of about 20-mm is recorded into 1024 channels.

TABLE 3

OTHER LINES

λ	ID	Multiplet	log $I(\lambda)/I(H\beta)$	
			M17-3	M17-14
4317 +4320	O II	(2)	p	p
4320 +4322	[Fe II]	(21F)(37F)		
4415 +4417	O II	(5)	−2.73 ± 0.08	−2.79 ± 0.08
4414 +4416	[Fe II]	(7F)(6F)		
4452	[Fe II]	(7F)	p	p
4452	O II	(5)		
4639 +4642	O II	(1)	−2.60 ± 0.07	−2.62 ± 0.07
4640	[Fe II]	(4F)		
4641 +4642	N III	(2)		
4649 +4651	O II	(1)	−2.69 ± 0.07	−2.73 ± 0.07
4647 +4650+4651	C III	(1)		
4674 +4676	O II	(1)	p	p
4686	He II		< −3.00	< −3.00

TABLE 4

EQUIVALENT WIDTHS[a]

λ	M17-3	M17-14
3835	25.7	35.5
4026	9.3	9.3
4102	114.8	147.9
4340	245.5	316.2
4387	3.0	3.5
4471	28.2	33.1
4713	4.2	4.5
4861	707.9	776.2
4922+30	10.7	10.7
5876	173.8	162.2
6563	3715.4	3388.4
6678	47.9	43.7
7065	66.1	43.7
7281	10.2	8.3

[a] In Angstroms.

TABLE 5

CONTINUUM OBSERVATIONS[a]

λ	$g(\lambda)$	M17-3	M17-14
3475	0.354	−1.99	−2.05
3525	0.343	−2.03	−2.08
3575	0.329	−2.04	−2.09
3625	0.315	−2.04	−2.08
3646^-	0.310	−2.04	−2.08
3646^+	0.310	−2.50	−2.61
3790	0.273	−2.54	−2.66
3890	0.245	−2.57	−2.69
4100	0.187	−2.65	−2.77
4200	0.162	−2.67	−2.80
4861	0.000	−2.85	−2.89

[a] log $i(\lambda)/I(\mathrm{H}\beta)$ in A^{-1}.

Two gratings were used that covered the following wavelength ranges: λλ3400-5200 and λλ5600-7400. The dual entrance slits used were 0.30 × 0.98 mm where the first value is along and the second is perpendicular to the dispersion; they correspond to 3.8″ × 12.4″ on the plane of the sky and their separation was 99″ , they were oriented east-west. The FWHM was of 3.8 channels and amounts to a resolution of 6.7 A. Each beam was treated independently and in all cases the sky was subtracted from the source. The sky measurements were made outside the body of M17. The coordinates of the observed positions are presented in Table 6.

The data were reduced to absolute fluxes using the standard stars observed by Stone (1977) and Oke (1974) and corrected for the nonlinearity of the detector by considering that the actual flux, F, is related to the instrumental signal, S, by (Peimbert & Torres-Peimbert 1987)

$$S \propto F^{1.07} \qquad (2$$

TABLE 6

POSITIONS, FLUXES AND REDDENING CORRECTIONS FOR THE KPNO OBSERVATIONS

Region	Position[a]		log	
	α	δ	$F(\mathrm{H}\beta)$	$C(\mathrm{H}\beta)$
M17-21	154″W	250″S	−12.67	2.15
M17-22	64 W	300 S	−12.40	1.60
M17-23	55 W	250 S	−11.92	1.70
M17-24	35 E	300 S	−11.89	1.30
M17-25	44 E	250 S	−12.28	1.40
M17-26	134 E	300 S	−12.21	1.10

[a] Relative to BD-16°4819.

The observed Hβ fluxes are presented in Table 6 Typical spectra gathered in a single night ar presented in Figure 5.

Based on the Balmer decrement, with the excep tion of Hα, and in the reddening law derived fron the CTIO observations presented in Table 2, we de rived the $C(\mathrm{H}\beta)$ values presented in Table 6. Sinc the blue and red part of the spectrum were not ob served simultaneously the $I(\mathrm{H}\alpha)/I(\mathrm{H}\beta)$ ratios wer adjusted to the theoretical one by applying a gra shift correction to the red part of the spectrum; th average gray shift was of 0.05 dex and it is partl due to small displacements of the entrance slits. I Table 7 we present the intrinsic line intensity ratios together with the 1 σ errors in the last digit. Th errors were estimated by comparing the results o the two observing seasons; again line intensity ratio with errors larger than 0.1 dex were not presented

III. TEMPERATURES AND DENSITIES

a) *Forbidden Lines*

The atomic parameters needed to derive th electron temperatures, the electron densities an the chemical abundances were taken from th compilation by Mendoza (1983). The electron tem peratures and densities are presented in Table 8 T_e(O III), T_e(N II) and T_e(S II) were derive from the following ratios: $I(4363)/I(5007)$, $I(5755)$ $I(6583)$ and $I(4068 + 4076)/I(6717 + 6731)$. Th T_e(S II) values were obtained under the assumptio that multiplet 10 of O II (λλ4069.6, 4069.9, 4072. and 4075.9) contributes with 25% to the liste

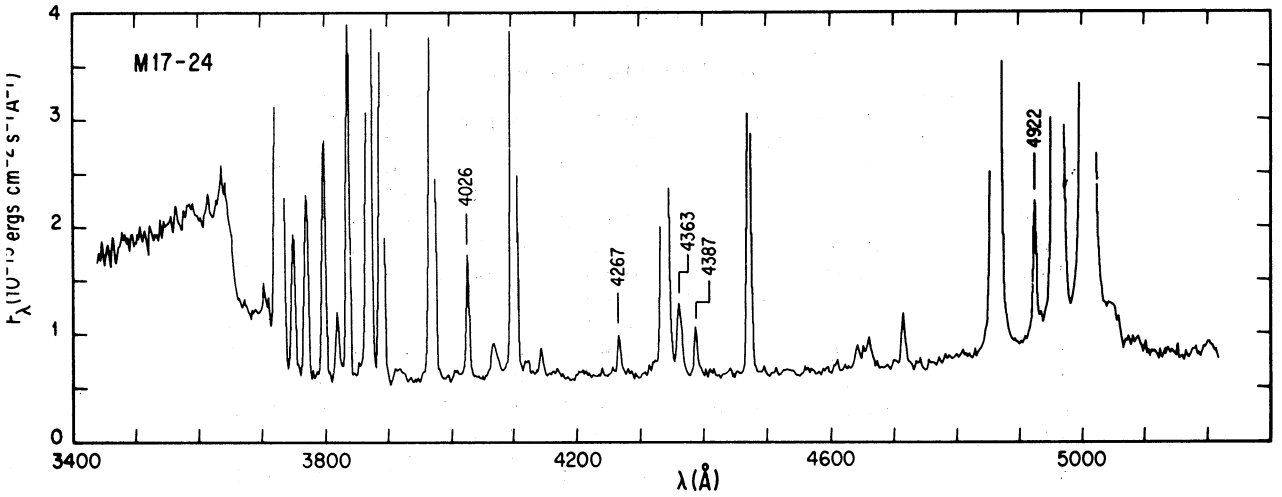

Fig. 5a. Blue spectrogram of M17-24, see Table 6.

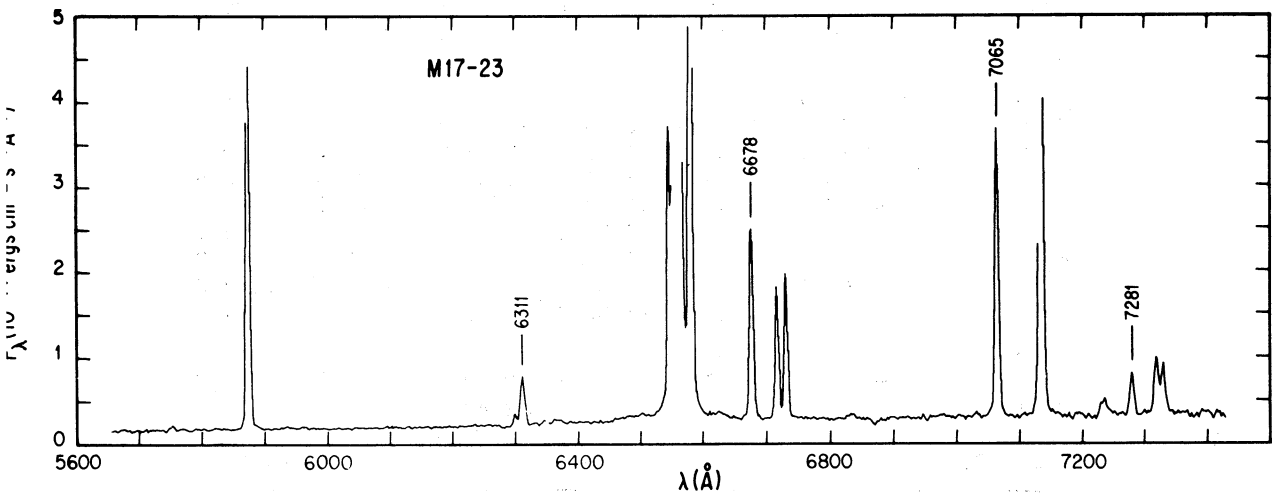

Fig. 5b. Red spectrogram of M17-23.

ntensity of $I(4068 + 4076)$; the S II temperatures were not used in the abundance determinations.

N_e(S II) and N_e(Cl III) were determined from he nebular ratios: $I(6717)/I(6731)$ and $I(5518)$ / (5538). For the abundance computations we dopted the N_e(S II) values; the only abundance atios that depend on N_e are $N(S^+)/N(H^+)$ and $N(O^+)/N(H^+)$, and the density dependence at the ensities presented in Table 8 is almost negligible.

b) *Balmer Continuum*

The Balmer continuum temperatures, T(Bac), were obtained from the ratio of the Balmer continuum, i(3646, Bac), to $I(H\beta)$. To estimate i(3646, Bac) it is necessary to determine the contribution of the other continua to the observed fluxes. For a pure nebular continuum this is done by subtracting the flux of the red side of the discontinuity $i(3646^+)$, from that of the violet side, $i(3646^-)$, since the intensity variation of the non-Balmer continua should be nil from $\lambda 3646^+$ to 3646^-. Nevertheless in the presence of a contribution to $i(\lambda)$ due to scattered starlight a small Balmer discontinuity in absorption is expected. Based on the spectral type of the brightest ionizing stars (O5), we have assumed that

$$i(3646, \mathrm{Bac}) = i(3646^-) - 0.94\, i(3646^+) \; ; \quad (3)$$

TABLE 7

LINE INTENSITIES FROM KPNO

λ	M17-21	M17-22	M17-23	M17-24	M17-25	M-17-26
3726+3729	-0.20 4	+0.11 3	-0.19 2	-0.14 2	+0.22 3	+0.46 3
3835	...	-1.13 3	-1.16 2	-1.15 2	-1.14 3	-1.15 3
3869	...	...	-0.62 2	-0.70 2	-0.75 3	-0.92 3
3889	-0.71 4	-0.67 3	-0.82 2	-0.79 2	-0.70 3	-0.81 3
3967+3970	-0.60 4	-0.66 3	-0.65 2	-0.68 2	-0.64 3	-0.79 3
4026	...	-1.59 5	-1.60 4	-1.68 4	-1.62 5	-1.74 5
4068+4076	...	...	-2.10 4	-2.01 4	-1.74 5	-1.66 5
4102	-0.59 2	-0.53 2	-0.58 1	-0.60 1	-0.60 1	-0.60 1
4267	...	...	-2.34 8	-2.24 8	-2.26 9	...
4340	-0.34 1	-0.34 1	-0.32 1	-0.33 1	-0.32 1	-0.34 1
4363	-1.89 7	...	-1.95 3	-1.96 4	...	-2.16 5
4472	...	-1.32 2	-1.29 1	-1.31 1	-1.30 2	-1.34 2
4658	...	...	-2.28 8	-2.26 8	...	...
4686	<-2.32	<-2.25	<-2.83	<-2.62	...	...
4713	...	...	-2.30 6	-2.20 5	...	...
4861	0.00	0.00	0.00	0.00	0.00	0.00
4922+4930	-1.88 5	-1.86 5	-1.88 3	-1.82 3	-1.89 4	-1.88 4
4959	+0.14 2	-0.06 2	+0.11 1	+0.07 1	+0.05 2	-0.09 2
5007	+0.66 2	+0.46 2	+0.59 1	+0.54 1	+0.51 1	+0.37 1
5198+5200	...	-2.25 9	...	-2.44 8	...	-2.33 9
5755	-2.46 9	...	-2.59 7	-2.75 9	-2.14 8	-1.98 8
5876	-0.81 3	-0.84 3	-0.80 2	-0.86 2	-0.82 2	-0.84 2
6300	-2.11 9	-1.80 8	-2.31 8	-2.35 8	-1.83 7	-1.80 7
6311	-1.78 6	-1.75 6	-1.85 4	-1.90 5	-1.76 5	-1.72 5
6563	+0.47 1	+0.47 1	+0.47 1	+0.47 1	+0.47 1	+0.47 1
6583	-0.70 2	-0.32 2	-0.71 2	-0.74 2	-0.32 2	-0.06 1
6678	-1.39 2	-1.40 2	-1.39 1	-1.40 2	-1.39 2	-1.40 2
6716	-1.61 4	-1.18 4	-1.61 2	-1.55 2	-1.16 3	-0.87 2
6731	-1.56 4	-1.10 4	-1.56 2	-1.53 2	-1.19 3	-0.91 2
7065	-1.30 4	-1.39 4	-1.31 2	-1.35 2	-1.39 3	-1.44 3
7136	-0.78 3	-0.82 3	-0.83 2	-0.89 2	-0.82 3	-0.85 3
7231+7236	...	...	-2.36 7	-2.40 7	...	...
7281	...	...	-2.18 5	-2.21 5	...	-2.22 6
7320+7330	-1.63 6	-1.51 5	-1.70 3	-1.73 3	-1.41 4	-1.28 4

the i(3646, Bac) values were derived by extrapolating the data in Table 5 and from equation (3). To derive the T_e(Bac) values we used the following equation (Peimbert 1971 and references therein)

$$T_e(\mathrm{Bac}) = 2.65 \left[\frac{i(\mathrm{Bac}, 3646)}{I(\mathrm{H}\beta)}\right]^{-1.52} . \quad (4)$$

In Table 9 we present the T_e(Bac) values for M17-3 and M17-14 where the adopted errors in the i(Bac, 3646)/I(Hβ) ratios are of 0.04 dex.

c) *Average Temperatures and Mean Temperature Variations*

For H II regions of uniform density and temperature and in the absence of observational errors all the solutions in the (N_e, T_e) diagram should intersect in only one point. In practice this is not the case; the expected error in the atomic parameter and in the observations are smaller than the differences among the different intersections. We consider that part of the difference is due to the presence of spatial temperature inhomogeneities along the line of sight.

In what follows we will define two different temperatures for each line of sight: one for the regions of high degree of ionization, T_e(O III) and another one for the regions of low degree of ionization, T_e(N II). Moreover we will define an average electron temperature, T_0, by

$$T_0(N_i, N_e) = \frac{\int T_e N_i N_e \, d\Omega dl}{\int N_i N_e d\Omega dl} , \quad (5$$

TABLE 8

TEMPERATURES AND DENSITIES

Reg.	T_e[N II]	T_e[O III]	N_e[S II]	N_e[Cl III]	T_e[S II]
1	11450 ± 600	8150 ± 200	600 ± 230	< 990	12700 ± 1000
2	11100 ± 550	8300 ± 200	720 ± 255	1170 ± 810	11300 ± 1000
3	11600 ± 550	8200 ± 150	845 ± 185	< 660	11800 ± 1000
4	9850 ± 500	8100 ± 150	920 ± 345	900 ± 720	12600 ± 900
5	8850 ± 400	8350 ± 150	735 ± 180	1000 ± 770	10100 ± 800
6	8900 ± 300	8450 ± 150	545 ± 140	1790 ± 850	8600 ± 600
11	9000 ± 400	8350 ± 200	800 ± 410	< 340	8600 ± 800
12	9900 ± 500	8250 ± 200	835 ± 430	< 660	11700 ± 1000
13	9250 ± 400	8000 ± 200	720 ± 280	< 150	12400 ± 800
14	9500 ± 400	7975 ± 200	605 ± 145	< 230	11400 ± 800
15	8900 ± 400	8100 ± 200	385 ± 110	< 900	8200 ± 400
21	10400 ± 900	8100 ± 300	895 ± 430	...	...
22	(9000)	(8350)	1310 ± 625	...	...
23	9300 ± 550	8150 ± 150	945 ± 205	...	12700 ± 1000
24	8400 ± 550	8350 ± 200	755 ± 185	...	15600 ± 1200
25	9850 ± 800	(8400)	400 ± 150	...	13300 ± 1500
26	9000 ± 600	8200 ± 250	345 ± 140	...	10100 ± 1000

TABLE 9

BALMER CONTINUUM TEMPERATURES, AVERAGE TEMPERATURES AND MEAN TEMPERATURE VARIATIONS

egion	T_e(Bac)	T_0	t^2
3	6100 $^{+\ 950}_{-\ 850}$	6600 ± 700	0.045 ± 0.019
14	6300 $^{+\ 1000}_{-\ 850}$	6700 ± 750	0.036 ± 0.020

here Ω is the observed solid angle and l is the istance along the line of sight; the root mean quare temperature variation, t, is given by

$$t^2 = \frac{\int T_e{}^2 N_i N_e \, d\Omega dl - T_0^2 \int N_i N_e \, d\Omega dl}{T_0^2 \int N_i N_e \, d\Omega dl} \quad . \quad (6)$$

can be shown that (Peimbert 1967)

$$T(\mathrm{Bac}) = T_0(1 - 1.70\, t^2) \ , \quad (7)$$

$$T_e(\mathrm{O\,III}) = T_0(\mathrm{h}) \left[1 + \frac{1}{2}\left(\frac{90800}{T_0(\mathrm{h})} - 3\right) t^2(\mathrm{h})\right] \ , \quad (8)$$

$$T_e(\mathrm{N\,II}) = T_0(\mathrm{l}) \left[1 + \frac{1}{2}\left(\frac{69000}{T_0(\mathrm{l})} - 3\right) t^2(\mathrm{l})\right] \ , \quad (9)$$

where T_0(h) and T_0(l) are the mean temperature in the regions of high and low degree of ionization.

It is possible to compute t^2(h) and T_0(h) from the T_e(Bac) and T(O III) values given in Tables 8 and 9 and from equations (7) and (8) under the assumption that T_e(Bac) is representative of the region where the [O III] lines originate; this is a reasonable assumption since in M17-3 more than 90% and in M17-14 more than 80% of the O atoms are in the O^{++} stage.

IV. CHEMICAL ABUNDANCES

a) *N, O, Ne, S, Cl, Ar and Fe*

To derive the ionic chemical abundances it has been assumed that there are two regions: a high ionization zone, where the O^{++}, Ne^{++}, S^{++}, Cl^{++}, Ar^{++} and Ar^{3+} lines originate, represented by T(O III) and a low ionization zone, where the N^+, O^+, S^+ and Fe^{++} lines originate represented by T(N II). In Table 10 it was assumed that there were no temperature inhomogeneities present, i.e., that $t^2 = 0.00$. In Table 11 it was assumed that $t^2 = 0.04$, for both the high and the low degree of ionization zones; equations (8) and (9) were used to determine T_0(h) and T_0(l). The T values for each line were derived from (Peimbert & Costero 1969)

$$T(\lambda_{nm}) =$$

$$= T_0\left\{1 + \left[\frac{(\Delta E/kT_0)^2 - 3\Delta E/kT_0 + 3/4}{\Delta E/kT_0 - 1/2}\right]\frac{t^2}{2}\right\}, \quad (10)$$

TABLE 10

IONIC ABUNDANCES FOR $t^2 = 0.00$[a]

Reg.	O^+	O^{++}	N^+	Ne^{++}	S^+	S^{++}	Cl^{++}	Ar^{++}	Ar^{3+}	Fe^{++}
1	-4.65	-3.49	-5.55	-4.21	-6.92	-5.06	-6.91	-5.61	-7.23	-6.49
2	-4.50	-3.53	-5.47	-4.26	-6.80	-5.10	-6.99	-5.63	-7.44	-6.55
3	-4.80	-3.53	-5.66	-4.25	-6.99	-5.12	-6.89	-5.64	-7.29	-6.76
4	-4.41	-3.54	-5.46	-4.25	-6.78	-5.14	-6.91	-5.65	-7.21	-6.43
5	-4.00	-3.63	-5.05	-4.39	-6.45	-5.12	-6.99	-5.66	-7.42	-6.20
6	-3.81	-3.69	-4.74	-4.52	-6.13	-5.08	-6.91	-5.65	-7.77	-5.88
11	-4.03	-3.66	-4.96	-4.43	-6.31	...	-6.94	-5.70	-7.66	-6.25
12	-4.40	-3.57	-5.28	-4.29	-6.67	-5.32	-6.94	-5.67	-7.46	-6.55
13	-4.40	-3.53	-5.33	-4.22	-6.71	-5.14	-6.90	-5.65	-7.42	-6.36
14	-4.27	-3.55	-5.34	-4.32	-6.58	-5.12	-6.92	-5.64	-7.47	-6.28
15	-3.82	-3.67	-4.77	-4.48	-6.05	-5.06	-6.84	-5.62	...	...
21	-4.66	-3.46	-5.48	-4.13	-6.90	-5.02	...	-5.58	...	...
22	-4.06	-3.71	-4.93	...	-6.29	-5.05	...	-5.66	...	...
23	-4.44	-3.54	-5.36	-4.22	-6.78	-5.10	...	-5.64	...	-6.38
24	-4.19	-3.63	-5.27	-4.35	-6.63	-5.20	...	-5.73	-7.30	-6.08
25	-4.18	-3.67	-5.04	-4.41	-6.49	-5.08	...	-5.66	...	...
26	-3.76	-3.77	-4.67	-4.53	-6.10	-4.98	...	-5.66	...	...

[a] In units of $\log N(X^{+m})/N(H^+) + 12$.

$$T(H\beta) = T_0\left(1 - \frac{1.90}{2}\, t^2\right) , \qquad (11)$$

where ΔE is the energy difference between the ground level and the excited level from which the emission line originates. The ionic abundances were derived from equations of the type

$$\frac{N(X^{+p})}{N(H^+)} \propto \frac{T(H\beta)^{-0.91}}{T(\lambda_{nm})^{-1/2}\, exp(-\Delta E/kT_{\lambda_{nm}})} \times \times \frac{I(X^{+p}, \lambda_{nm})}{I(H\beta)} . \qquad (12)$$

To derive the total O abundance the following equation was used (Peimbert & Costero 1969)

$$\frac{N(O)}{N(H)} = \frac{N(O^+) + N(O^{++})}{N(H^+)} . \qquad (13)$$

The total abundances are presented in Figure 6 for two values of t^2 and as a function of $\log (O^+/O^{++})$. For a given t^2 value the dispersion in O/H is very small which implies that t^2 and the fraction of O atoms embedded in dust grains are fairly independent of O^+/O^{++}, i.e., the line of sight.

To derive the total abundances of the other elements it is necessary to estimate the fraction of ions present in unobserved stages of ionization, i.e., the ionization correction factors, i_{cfs}. This estimate can be done by means of ionization structure models or by empirical means. The combination of these two methods, with the condition that all the observed lines of sight should yield the same abundance made possible to estimate the i_{cfs}.

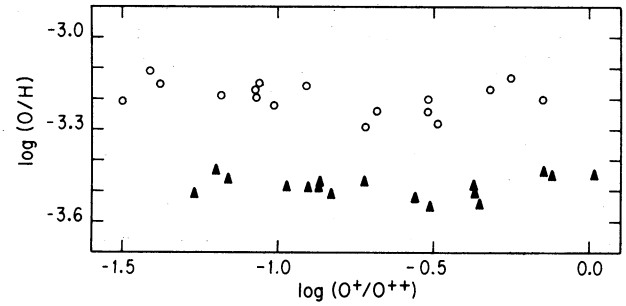

Fig. 6. Total O abundances as a function of degree of ionization. The triangles correspond to $t^2 = 0.00$, the circles to $t^2 = 0.04$.

Mathis & Rosa (1991) have computed ionization correction factors for multiple lines of sight, within a particular object, based on atmospheric models by Kurucz (1979). They have computed two sets of coefficients: for cool atmospheres and for hot atmospheres. For a cool atmosphere log

TABLE 11

IONIC ABUNDANCES FOR $t^2 = 0.04$[a]

Reg.	O^+	O^{++}	N^+	Ne^{++}	S^+	S^{++}	Cl^{++}	Ar^{++}	Ar^{3+}	Fe^{++}
1	-4.55	-3.17	-5.46	-3.86	-6.83	-4.70	-6.60	-5.35	-6.96	-6.41
2	-4.40	-3.22	-5.37	-3.92	-6.73	-4.75	-6.69	-5.38	-7.18	-6.46
3	-4.71	-3.21	-5.58	-3.91	-6.90	-4.77	-6.58	-5.39	-7.02	-6.67
4	-4.28	-3.21	-5.34	-3.89	-6.66	-4.77	-6.59	-5.38	-6.94	-6.31
5	-3.83	-3.32	-4.90	-4.06	-6.30	-4.78	-6.70	-5.41	-7.16	-6.05
6	-3.64	-3.39	-4.59	-4.19	-5.98	-4.75	-6.63	-5.41	-7.52	-5.74
11	-3.87	-3.35	-4.82	-4.10	-6.17	...	-6.65	-5.45	-7.40	-6.10
12	-4.26	-3.25	-5.15	-3.95	-6.55	-4.96	-6.64	-5.42	-7.20	-6.43
13	-4.25	-3.19	-5.19	-3.86	-6.57	-4.76	-6.58	-5.38	-7.14	-6.22
14	-4.12	-3.21	-5.21	-3.96	-6.46	-4.74	-6.60	-5.37	-7.18	-6.16
15	-3.66	-3.34	-4.62	-4.12	-5.90	-4.69	-6.53	-5.35	...	...
21	-4.54	-3.13	-5.37	-3.77	-6.79	-4.65	...	-5.31	...	...
22	-3.89	-3.40	-4.78	...	-6.14	-4.71	...	-5.41	...	...
23	-4.29	-3.22	-5.22	-3.87	-6.64	-4.74	...	-5.38	...	-6.24
24	-4.00	-3.32	-5.10	-4.02	-6.47	-4.86	...	-5.48	-7.04	-5.92
25	-4.05	-3.37	-4.92	-4.09	-6.37	-4.74	...	-5.42	...	...
26	-3.60	-3.45	-4.53	-4.19	-5.96	-4.63	...	-5.41	...	...

[a] In units of $\log N(X^{+m})/N(H^+) + 12$.

$(O^+/O^{++}) > 1.144 + 1.272 \log (S^+/S^{++})$ while for a hot atmosphere $\log (O^+/O^{++}) < 1.144 + 1.272 \log (S^+/S^{++})$. In Figure 7 we have plotted $\log (O^+/O^{++})$ versus $\log (S^+/S^{++})$ for the observed points in M17; also in this figure we have drawn the predictions made by Mathis & Rosa based on three Kurucz atmospheres; the observed points follow quite closely the model for 40 000 °K and $\log g = 4.0$ and are very close to the dividing line between cool and hot atmospheres.

In Figure 8 we show the O^+/O^{++} versus N^+/O^+ diagram, there is considerable scatter that we attribute to possible errors in the electron temperature and to differences between the oxygen and nitrogen ionization degrees (i.e., between O^+/O and N^+/N). Peimbert & Costero (1969) suggested the following equation to estimate the N abundance

$$\frac{N(N)}{N(H)} = i_{cf}(N)\,\frac{N(N^+)}{N(H^+)} = \frac{N(O)}{N(O^+)}\,\frac{N(N^+)}{N(H^+)} \cdot (14)$$

This equation is a very good approximation for H II regions with relatively low degree of ionization, while for H II regions of high degree of ionization there are zones where N^{++} and O^+ coexist and equation (14) yields only a lower limit to the N/H ratio.

In Table 12 we present three sets of N/H ratios

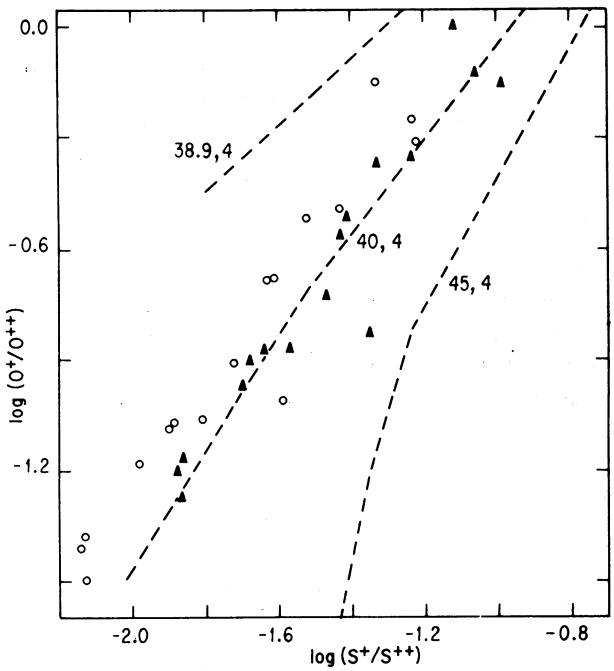

Fig. 7. Comparison of ionization structure models with observations in the $N(O^+)/N(O^{++})$ versus $N(S^+)/N(S^{++})$ diagram, symbols as in Figure 6. The dashed lines correspond to ionization structure models by Mathis & Rosa (1991) based on atmospheres by Kurucz (1979) for $\log g = 4.0$ cm s^{-2} and $T^* = 38\,900$ K, 40 000 K and 45 000 K.

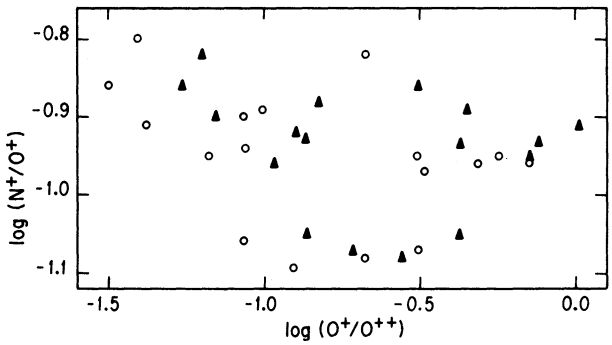

Fig. 8. $N(N^+)/N(O^+)$ as a function of ionization degree, symbols as in Figure 6.

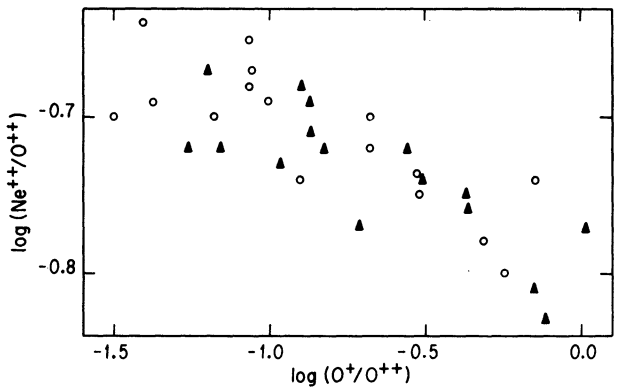

Fig. 9. $N(Ne^{++})/N(O^{++})$ as a function of ionization degree, symbols as in Figure 6.

for different i_{cf}(N): a) from the cool atmospheres by Mathis & Rosa (1991), b) from the hot atmospheres by Mathis & Rosa and, c) from equation (14). The adopted values are an average of the cool and hot atmospheres results; notice that the adopted values are from 0.13 to 0.16 dex higher than those derived from equation (14). Also in Table 12 we present the average abundances for the four regions of lowest degree of ionization, i.e., those with the lowest i_{cf}(N); these average values are practically indistinguishable from those derived for the whole sample.

To estimate the Ne abundance the following equation has been used often (e.g., Peimbert & Costero 1969)

$$\frac{N(\mathrm{Ne})}{N(\mathrm{H})} = \frac{N(\mathrm{O}^+ + \mathrm{O}^{++})}{N(\mathrm{O}^{++})} \frac{N(\mathrm{Ne}^{++})}{N(\mathrm{H}^+)} \cdot \qquad (15)$$

Equation (15) provides a very good approximation for the $i_{cf}(Ne^{++})$; there are two cases where equation (15) is no longer applicable: a) for regions where a large fraction of H^0 is present the charge exchange reaction $O^{++} + H^0 \rightarrow O^+ + H^+$ allows some O^+ to coexist with Ne^{++} and equation (15) yields an upper limit to the real value (e.g., Pequignot 1980 and references therein), b) for objects of low degree of ionization where a small fraction of Ne^+ coexists with O^{++}, equation (15) becomes a lower limit to the real value. In Figure 9 we present the O^+/O^{++} versus Ne^{++}/O^{++} diagram where it can be seen that the higher the ionization degree the higher the Ne^{++}/O^{++} ratio. This result implies that the second case mentioned above dominates and that the best N(Ne)/N(H) values are provided by the regions of high degree of ionization. From Tables 10 and 11, Figure 9 and equation (15) we adopt the values derived from the average of regions 1, 2, 3 and 23, these values are presented in Table 13. Notice that the i_{cf} derived by Mathis and Rosa, that are also presented in Table 13, are almost identical to those derived from equation (15).

In Figure 10 we present the O^+/O^{++} versus S^{++}/H^+ diagram. The points indicate the S^{++}/H^+ abundances, while the arrows include the contribution due to S^+/H^+; for the points without arrows

TABLE 12

TOTAL NITROGEN ABUNDANCES[a]

Method	$t^2 = 0.00$		$t^2 = 0.04$	
	⟨ all ⟩	⟨ 6, 15, 22, 26 ⟩	⟨ all ⟩	⟨ 6, 15, 22, 26 ⟩
cool	−4.33	−4.33	−4.06	−4.09
hot	−4.26	−4.24	−3.92	−3.96
eq. 14	−4.42	−4.39	−4.15	−4.18
⟨ cool, hot ⟩	−4.29	−4.29	−3.99	−4.03

[a] Given by log N(N)/N(H).

TABLE 13

TOTAL NEON ABUNDANCES[a]

Method	$t^2 = 0.00$		$t^2 = 0.04$	
	⟨ all ⟩	⟨ 1, 2, 3, 23 ⟩	⟨ all ⟩	⟨ 1, 2, 3, 23 ⟩
cool	−4.21	−4.19	−3.90	−3.86
hot	−4.20	−4.20	−3.88	−3.88
eq. 15	−4.23	−4.20	−3.90	−3.87

[a] Given by log N(Ne)/N(H).

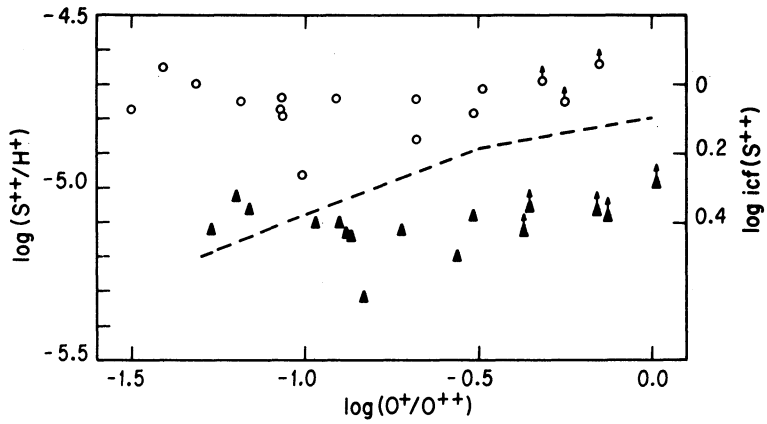

Fig. 10. Left hand vertical axis: $N(S^{++})/N(H^+)$ as a function of ionization degree, symbols as in Figure 6. Arrows indicate $N(S^+ + S^{++})/N(H^+)$ values in units of the left hand vertical axis; symbols without arrows indicate that the contribution of S^+ to the $N(S^+ + S^{++})/N(H^+)$ is negligible. Right hand vertical axis and dashed line indicate the predicted $i_{cf}(S^{++})$ value from the $T^* = 41\,200$ K Kurucz model (Mathis & Rosa 1991) as a function of ionization degree.

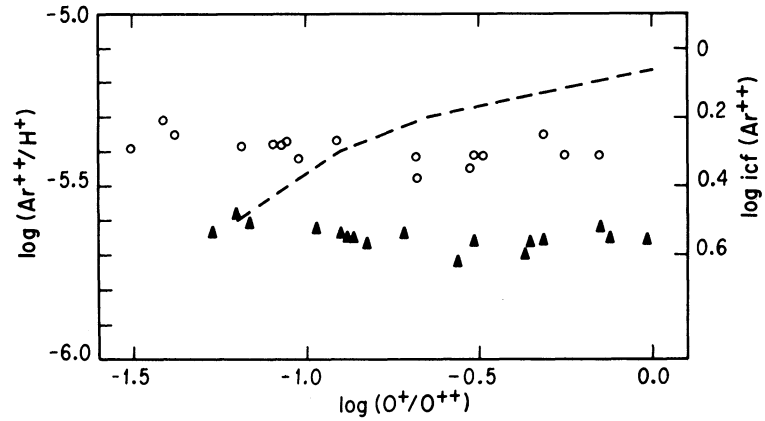

Fig. 11. Left hand vertical axis: $N(Ar^{++})/N(H^+)$ as a function of ionization degree, symbols as in Figure 6. Right hand vertical axis and dashed line indicate the predicted $i_{cf}(Ar^{++})$ value from the $T^* = 41\,200$ K Kurucz model (Mathis & Rosa 1991) as a function of ionization degree.

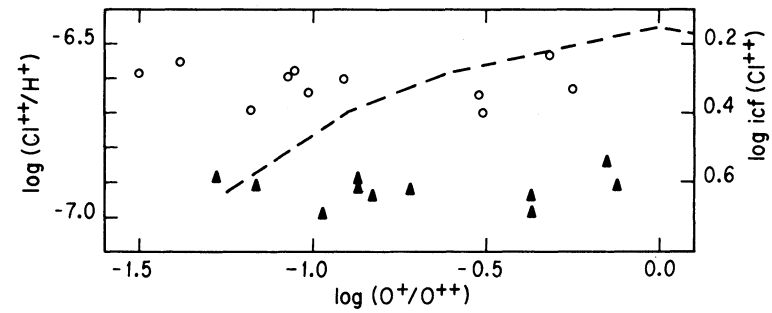

Fig. 12. Left hand vertical axis: $N(Cl^{++})/N(H^+)$ as a function of ionization degree, symbols as in Figure 6. Right hand side vertical axis and dashed line indicate the predicted $i_{cf}(Cl^{++})$ value from the $T^* = 41\,200$ K Kurucz model (Mathis & Rosa 1991) as a function of ionization degree.

the S^+/H^+ contribution is negligible. On the right vertical axis we present the $i_{cf}(S^{++})$ derived by Mathis & Rosa (1991) from the atmosphere by Kurucz for $T^* = 41\,200$ °K and log $g = 4.0$; on the left hand side of the diagram the $i_{cf}(S^{++})$ becomes larger because most of the sulphur becomes S^{3+} while the contribution to the i_{cf} in the right hand side is due to S^+. Therefore to minimize the uncertainty of the possible S^{3+} contribution we will adopt the average value of $(S^+ + S^{++})/H^+$ for the four regions with the lowest degree of ionization (regions 6, 15, 22 and 26) as representative of the total S/H value; these values are presented in Table 18. The S^{++}/H^+ versus O^+/O^{++} distribution does not indicate the presence of appreciable amounts of S^{3+} even for the regions with the highest degree of ionization (see also the discussion on Ar below).

In Figure 11 we present the O^+/O^{++} versus Ar^{++}/H^+ diagram. On the right vertical axis we present the $i_{cf}(Ar^{++})$ derived by Mathis & Rosa (1991) from the atmosphere by Kurucz for $T^* = 41\,200$ °K and log $g = 4.0$. On the left hand side of the diagram the $i_{cf}(Ar^{++})$ becomes larger because most of the Ar becomes Ar^{3+} while the contribution to the i_{cf} in the left hand side is due to Ar^+. From the determinations in Tables 10 and 11 it follows that the fraction of Ar in the form of Ar^{3+} is almost negligible. To minimize the contribution of the unobserved Ar^+ ions we have adopted the average value of $(Ar^{++} + Ar^{3+})/H^+$ for the four well observed regions with the highest degree of ionization (1, 2, 3 and 4) as representative of the total Ar/H ratio. These values are presented in Table 18.

The very low observed Ar^{3+}/Ar^{++} ratio indicates the presence of one of the following alternatives or a combination of them: a) since we are observing only a fraction of the H II region it is possible that we could be missing the Ar^{3+} and S^{3+} region predicted by the ionization structure models of Kurucz, the main ionizing stars proposed are to the west and south of the observed regions (Felli *et al.* 1984), b) the flux of the ionizing stars beyond 40.7 eV is smaller than that predicted by Kurucz models, for both hot and cool models and c) there is dust absorption of high energy photons inside the H II region. It is beyond the scope of this study to produce an ionization structure model to explore these possibilities further.

In Figure 12 we present the O^+/O^{++} versus Cl^{++}/H^+ diagram from Tables 10 and 11 and the O^+/O^{++} versus $i_{cf}(Cl^{++})$ diagram from Mathis & Rosa (1991). Considering the similar ionization potentials of S, Cl and Ar, and Figure 12 we estimate that most Cl atoms are in the form of Cl^{++}. The total abundances presented in Table 18 were derived from the Cl^{++} average for all the observed regions and adopting $i_{cf}(Cl^{++}) = 0.1$ dex.

In Figure 13 we present the Fe^{++}/H^+ versus O^+/O^{++} diagram. There is a very strong correlation in the sense that the lower the degree of ionization the higher the Fe^{++}/H^+ ratio. Under the assumption that Fe/H should be constant over the different lines of sight, and considering the similarity of the N^+ and Fe^{++} ionization potentials we propose that

$$\frac{N(\mathrm{Fe})}{N(\mathrm{H})} = i_{cf}(\mathrm{Fe}^{++})\,\frac{N(\mathrm{Fe}^{++})}{N(\mathrm{H}^+)} = \frac{N(\mathrm{N})}{N(\mathrm{N}^+)}\,\frac{N(\mathrm{Fe}^{++})}{N(\mathrm{H}^+)}\,. \qquad (16)$$

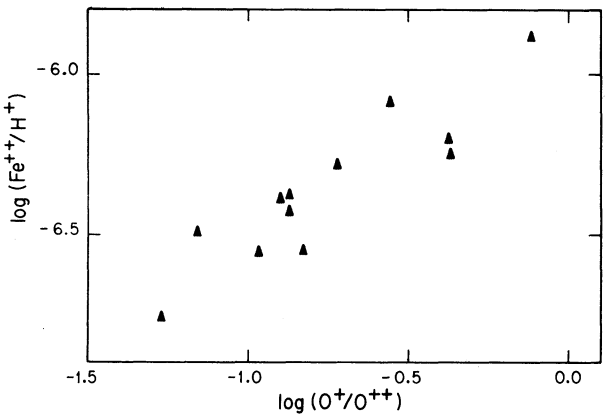

Fig. 13. $N(Fe^{++})/N(H^+)$ as a function of ionization degree, symbols as in Figure 6.

In Figure 14 we present the Fe^{++}/H^+ versus N^+/N diagram where there is a strong linear correlation between these two quantities in agreement with the Fe^{++} i_{cf} proposed in equation (16).

In Table 18 we present the average value for all the observed regions based on equation (16), Tables 10 and 11 and the $i_{cf}(N^+)$ values from the work by Mathis & Rosa (1991).

The Fe/H value derived from the Fe^{++}/H^+ determination by Osterbrock, Tran, & Veilleux (1992) and equation (16) is in excellent agreement with the Fe/H abundance derived by Osterbrock *et al.* from their observations and an ionization correction factor provided by photoionization models.

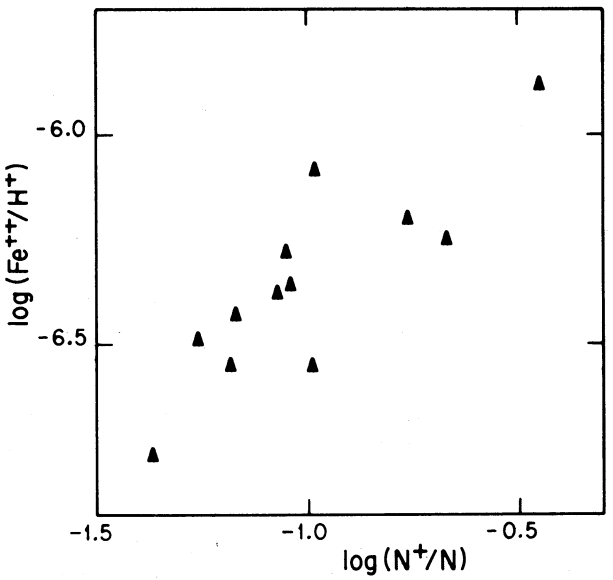

Fig. 14. $N(Fe^{++})/N(H^+)$ as a function of $N(N^+)/N(N)$, symbols as in Figure 6.

b) *He from Optical Data*

In Table 14 we present the He^+/H^+ abundances based on the computations by Smits (1991) and Hummer and Storey (1987) for $t^2 = 0.00$ and without considering collisional excitations nor self-absorption from the 2^3S level; we label these abundances $t^2 = 0.00$ (uncorrected). If the computations by Brocklehurst (1972) are used instead of those by Smits (1991) the abundances in Table 14 have to be multiplied by 1.00, 0.98 and 0.99 for λλ4472, 5876 and 6678 respectively.

To correct for collisional excitation from the 2^3S level, we used the computations by Smits (1991), the increase in the line intensities amounts to factors of about 1.006, 1.01, 1.004 and 1.12 for λλ4472, 5876, 6678 and 7065 respectively; similar results for λλ4472, 5876 and 6678 are obtained from the computations by Clegg (1987) and Peimbert & Torres-Peimbert (1987).

To apply a correction for self-absorption we used the $I(7065)/I(6678)$ ratio after correcting it

TABLE 14

IONIC HELIUM ABUNDANCES[a]

	(uncorrected)				(corrected)			
Region	4472	5876	6678	7065	4472	5876	6678	$\langle He^+/H^+ \rangle$
				$t^2 = 0.00$				
1	100	112	101	244	99	109	101	103
2	103	113	97	226	102	110	96	103
3	103	112	104	227	102	109	103	105
4	103	109	98	213	102	107	98	102
5	105	108	99	197	104	105	99	103
6	98	106	100	171	98	104	99	100
11	98	105	93	201	97	103	92	97
12	101	107	92	184	100	106	92	99
13	98	107	98	200	97	104	98	100
14	96	106	98	173	95	105	98	99
15	96	105	96	144	95	103	96	98
21	...	112	103	233	...	109	103	105
22	96	105	102	188	95	103	101	100
23	103	115	103	228	102	112	103	106
24	98	101	102	206	97	98	101	99
25	101	110	104	188	100	108	104	104
26	91	105	101	168	91	103	101	98
< >	99	107	100	...	99	106	99	...
				$t^2 = 0.04$				
< >	96	101	93	...	95	99	93	...

[a] Given by $10^3 \times N(He^+)/N(H^+)$.

for collisional excitation and compared it with the recombination prediction, the excess ratio was used to estimate the optical depth in λ7065 based on the computations by Robbins (1968) normalized to the maximum values for total self-absorption presented by Cox & Daltabuit (1971). The corrections amounted to factors in the 1.003 to 1.02 range for $y^+(5876)$ and in the 1.001 to 1.006 range for $y^+(4472)$, where

$$y^+(\lambda) = \frac{N(He^+, \lambda)}{N(H^+)} , \qquad (17)$$

the results are presented in Table 14. In general the optical thickness of M17 increases from east to west as can be seen from the $y^+(7065)$ values presented in Table 14. The self-absorption correction for λ6678 is negligible (Robbins & Bernat 1973).

The uncorrected $y^+(5876)$ values are systematically higher than $y^+(4472)$ and $y^+(6678)$. The differences become smaller for the corrected values and for $t^2 = 0.04$, if the computations by Brocklehurst (1972) are used the differences become smaller. Part of these systematic effects could be due to the adopted reddening law.

The total helium abundance in an H II region is given by

$$\frac{N(He)}{N(H)} = \frac{N(He^0 + He^+ + He^{++})}{N(H^+)} \qquad (18)$$

From the computations by Hummer and Storey (1987) and the $I(4686)/I(H\beta)$ upper limit in Table 3 it is found that $N(He^{++})/N(H^+) < 8 \times 10^{-5}$ which is a negligible amount. On the other hand, the amount of neutral helium is not negligible; in

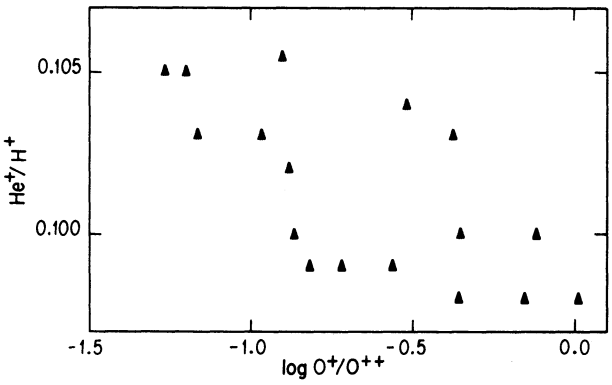

Fig. 15. $N(He^+)/N(H^+)$ as a function of ionization degree, symbols as in Figure 6.

Figure 15 it can be seen that the larger the O^+/O^{++} values the smaller the He^+/H^+ values indicating the presence of neutral helium. A similar decrease is observed in the Ne^{++}/O^{++} values with increasing O^+/O^{++} values (see Figure 9).

In Table 15 we have divided all the observed regions in three groups according to their O^+/O^{++} ratios. The group with the highest degree of ionization shows the highest He^+/H^+ values. We also present in Table 15 the radiation softness parameter, η, defined as (Vílchez & Pagel 1988)

$$\eta = (O^+/S^+)(S^{++}/O^{++}) . \qquad (19)$$

Pagel *et al.* (1992) have pointed out that for $\log \eta < 0.9$ the amount of He^0 inside H II regions for a wide variety of models is negligible; while for $\log \eta > 1$ it is large and model dependent. It can be seen from Table 15 that the smaller the η value the higher the He^+/H^+ value.

TABLE 15

AVERAGE IONIC AND TOTAL HELIUM ABUNDANCES[a] AND RADIATION SOFTNESS PARAMETER

Regions	$t^2 = 0.00$			$t^2 = 0.04$		
	$\langle He^+/H^+ \rangle$	$\langle He/H \rangle$	$\langle \log \eta \rangle$	$\langle He^+/H^+ \rangle$	$\langle He/H \rangle$	$\langle \log \eta \rangle$
1, 2, 3, 21, 23	0.104	0.106	0.68	0.099	0.100	0.75
4, 12, 13, 14, 24, 25	0.100	0.103	0.75	0.094	0.097	0.81
5, 6, 11, 15, 22, 26	0.099	0.106	0.95	0.093	0.099	1.00

[a] By number.

To estimate the amount of He^0 we will assume that He is neutral in the regions where S in once ionized, i.e.,

$$\frac{N(He^0)}{N(He)} = \frac{N(S^+)}{N(S)} \quad . \tag{20}$$

Therefore

$$\frac{N(He)}{N(H)} = i_{cf}(He^+)\,\frac{N(He^+)}{N(H^+)} =$$

$$= \left[1 + \frac{N(S^+)}{N(S) - N(S^+)}\right] N(He^+) \quad . \tag{21}$$

For the He/H ratio we will take the average of regions 1, 2, 3, 21 and 23 that show the smallest i_{cf}. We consider that equation (20) is adequate because the He/H ratio is no longer dependent on η or O^+/O^{++}.

c) *He from Radio Data*

In Table 16 and Figure 16 we present some of the best He^+/H^+ determinations based on radio data for M17S. Most of the efforts in the radio region have been devoted to M17S, because it is brighter than M17N, while all of the efforts in the optical region have been devoted to M17N, because M17S is heavily obscured by dust. Both M17S and M17N belong to the same H II region complex (e.g., Felli *et al.* 1984) and are expected to have the same chemical composition.

From the values in Table 16 and Figure 16 it can be seen that there is a trend in the He^+/H^+ ratios in the sense that the higher the n value the smaller

TABLE 16

$N(He^+)/N(H^+)$ VALUES FOR M17S DERIVED FROM RADIO DATA

Line	HPBW	He^+/H^+	Source
41α	18″	0.122 ± 0.024	1
53α	39	0.108 ± 0.004	1
76α	138	0.097 ± 0.005	2
86α	210	0.102 ± 0.005	3
91α	192	0.090 ± 0.013	4
109α	144	0.093 ± 0.003	5
114β	192	0.090 ± 0.011	3
130γ	192	0.091 ± 0.011	3

(1) Peimbert *et al.* 1988; (2) McGee & Newton 1981; (3) Lichten *et al.* 1979; (4) Peimbert *et al.* 1992; (5) Churchwell *et al.* 1978.

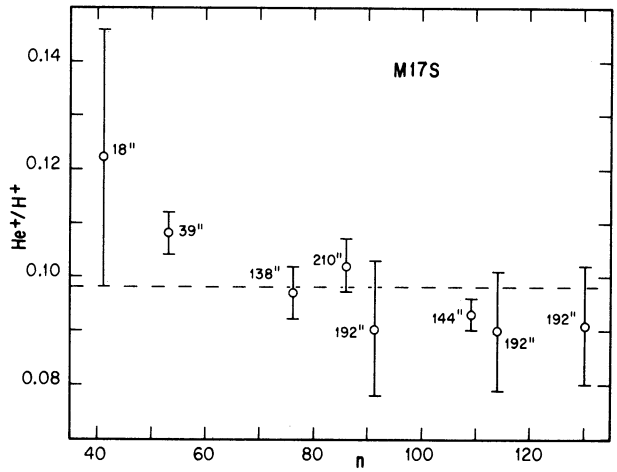

Fig. 16. $N(He^+)/N(H^+)$ as a function of principal quantum number, n, see Table 16.

the He^+/H^+ ratio. Other H II regions also show this trend (e.g., Peimbert *et al.* 1992 and references therein); there are different explanations for this behaviour, the main ones are: a) that it is a beam size effect-produced by the smaller size of the He^+ ionized zone than the H^+ one, as is the case in the Orion nebula (e.g., Peimbert *et al.* 1988), b) that for intermediate n values the H lines are closer to case A than the He I lines while for high n values both H I and He I lines approach case B (Ferland & Cota 1988; Baldwin *et al.* 1991). This second suggestion might not be correct; although it is true that the deviations of the H I lines from case B toward case A are higher at intermediate n values ($40 \leq n \leq 60$ for $N_e = 10^3$ cm^{-3}) than at high n values (Hummer & Storey 1992), it is not obvious that at intermediate n values the H I lines are closer to case A than the He I lines. In what follows we will discuss this issue.

There are two classic cases for the behavior of the hydrogen recombination lines that are well studied: case A where all Lyman line photons escape the nebula, or are absorbed by dust; and case B, where the nebula is optically thick to Lyman line emission, and, with the exception of the Lyman α photons, each of the other Lyman photons is eventually converted by scattering into a Lyman α plus a Balmer line photon that escapes the nebula (Baker & Menzel 1938). Therefore case B produces higher emissivities than case A for the recombination lines that end at n values higher than unity. To study the H line emissivities under cases A and B it is necessary to compute the b_n values, the departure coefficients from the Saha-Boltzmann populations.

Hummer & Storey (1992) have found that at $N_e = 10^4$ cm^{-3} the difference in the emissivities between cases A and B reaches a maximum in the $30 \leq$

$n \leq 50$ range where l changing collisions for a given n value become important. For the $10 \leq n \leq 20$ range the absence of l changing collisions reduces the relative importance of the $n_p \rightarrow 1s$ transition and the difference in emissivities between cases A and B becomes smaller than in the $30 \leq n \leq 50$ range. For $n \geq 70$ collisional ionization and three body recombination become important,

$$H(n) + e \rightleftarrows H^+ + e + e \ ,$$

these processes directly link the bound states with the free-electron states and both cause the b_n factors to tend to unity; therefore cases A and B tend to converge and the excess emissivity of case B relative to case A becomes negligible (Seaton 1964; Hummer & Storey 1992).

The He I singlets can be approximated by cases A and B, just like H I, because the ground state is a singlet, therefore to a first approximation the H I and He I singlets behave similarly. For He I triplets there is no case B because 2^3S is the lowest level, therefore the emissivity of the He I triplets is not increased by transitions from the $n = 1$ level and there is only the pure recombination case that corresponds to case A. Therefore, contrary to the suggestion by Ferland & Cota (1988) and Baldwin *et al.* (1991), that consider that the He I triplets behave like case B at intermediate n values, we consider that they behave like case A and that the helium to hydrogen intensity ratios should *increase* with n value due to this effect. Accurate computations for the He I emissivities are needed to quantify this effect.

Peimbert *et al.* (1992) from 91α, 114β and 130γ observations of a group of galactic H II regions made with approximately the same beam size did not find evidence, at the 10% level, for an increase or decrease of the He^+/H^+ ratio with n value.

In radio determinations of He^+/H^+ values the same emissivity has been assumed for the He I and H I recombination lines that originate in the same n level, and consequently that

$$\frac{N(He^+)}{N(H^+)} = \frac{I(He^0, n\alpha)}{I(H^0, n\alpha)} \qquad (22)$$

How large and in which sense are the deviations caused by intermediate situations between cases A and B? There are two extreme situations: a) when the H I lines are in case A the He I lines are also in case A and equation (22) is correct; b) when the H I lines are in case B, the He I singlets are also in case B and the He I triplets in case A. Since about one fourth of the recombinations go to singlet states and three fourths go to triplet states, the He I emissivities are reduced by 3/4 of the difference between cases A and B. From the computations by Hummer & Storey (1992) the maximum reduction in the emissivities of H I between cases A and B for $n > 10$ amounts to 15%, which for $10^2 < N_e < 10^4$ cm^{-3} corresponds to $30 < n < 50$, therefore 3/4 of this difference corresponds to a maximum reduction of 11% for the He I emissivities. For higher n values ($n > 50$) and for intermediate situations between case A and case B for the H I lines the reduction of the He I line emissivities are considerably smaller than 11% and equation (22) yields slightly lower $N(He^+)/N(H^+)$ ratios than the real ones.

The weighted average of all the $N(He^+)/N(H^+)$ values in Table 16 yields 0.098 ± 0.002. If only the observations with $n \geq 76$ were used we would obtain 0.095 ± 0.002.

The 53α $N(He^+)/N(H^+)$ value of 0.108 ± 0.004 is higher than the average value for $n \geq 76$, 0.095 ± 0.002. The difference is in the opposite direction to that expected in the presence of deviations from case A, therefore we consider that most of the difference is due either to observational errors or to beam size effects.

Based on infrared observations of [Ne II] and [S IV] lines in M17S it has been found that the most highly ionized material lies in the region comprised by the 39″ beam size of the 53α observations and that in this region the He^+ and H^+ Stromgren spheres coincide (Lester *et al.* 1983), from these considerations we would expect a very small correction for the presence of neutral helium inside the brightest parts of M17S. If there were a He^0 zone inside the H II region, the He^+/H^+ values derived from smaller size beams centered in the brightest areas would be higher and closer to the $N(He)/N(H)$ value.

The total He to H ratio in an H II region ionized by stars of spectral type O5 and later is given by equation (18). The difference between the 53α value and the average $n \geq 76$ value could be due to a higher amount of neutral helium in the outer parts of M17S than in the central parts, (what we have referred as to a beam size effect). If this were the case the $N(He)/N(H)$ ratio would be close to the 53α determination (i.e., 0.108 ± 0.004). On the other hand if the amount of neutral helium in the different beam sizes were the same, then the $N(He^+)/N(H^+)$ ratio would be the weighted average of all the observations, i.e., 0.098 ± 0.002. Note that the corrections both for neutral helium and for deviations from case A of the H I lines and the He I singlets are in the direction of increasing the $N(He)/N(H)$ value. We expect both effects to be small and conclude from

the radio data that for M17S $0.108 \geq N(\mathrm{He})/N(\mathrm{H}) \geq 0.098$ and consequently that $N(\mathrm{He})/N(\mathrm{H}) = 0.103 \pm 0.005$, in excellent agreement with the optical determinations.

d) *Carbon*

The C^{++}/H^+ ratios were derived from the C II 4267 A recombination line using the following equation (Seaton 1978; Hummer & Storey 1987),

$$\frac{N(C^{++})}{N(H^+)} = 0.109 \left(\frac{T}{10^4}\right)^{0.14} \frac{I(4267)}{I(H\beta)} \qquad (23)$$

The results are presented in Figure 17 and Table 17. There is no clear cut tendency in Figure 17 between the C^{++}/H^+ abundance and the O degree of ionization, which means that the fractions of C^+/H^+ and C^{3+}/H^+ are smaller than the C^{++}/H^+ observational errors. From the ionization potentials of C^{++} and Ar^{++} (47.9 and 40.7 eV) and considering that the Ar^{3+}/Ar^{++} ratio is very small, the expected C^{3+}/C^{++} ratio is negligible.

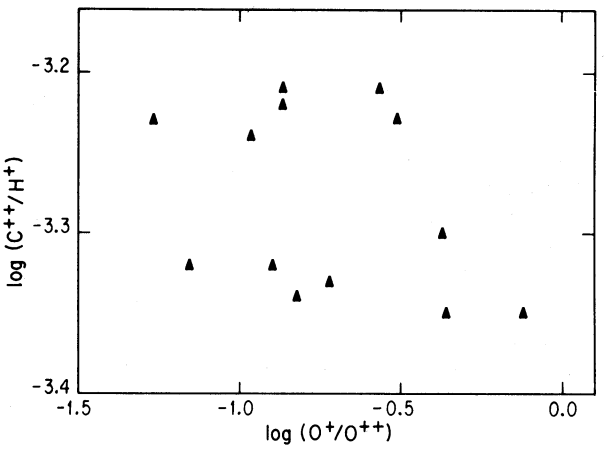

Fig. 17. $N(C^{++})/N(H^+)$ as a function of ionization degree, symbols as in Figure 6.

TABLE 17

IONIC AND TOTAL CARBON ABUNDANCES[a]

Regions	$t^2 = 0.00$		$t^2 = 0.04$	
	$\langle C^{++}/H^+ \rangle$	$\langle C/H \rangle$	$\langle C^{++}/H^+ \rangle$	$\langle C/H \rangle$
1,2,3,21,23	−3.28	−3.27	−3.29	−3.28
4,12,13,14,24,25	−3.26	−3.25	−3.27	−3.26
5,6,11,15,22,26	−3.33	−3.31	−3.34	−3.33
all	−3.27	−3.26	−3.28	−3.27

[a] Logarithmic ratios by number.

On the other hand the ionization potential of C^+ is intermediate between those of S^+ and He^0 (24.4, 23.3 and 24.6 eV respectively), therefore we expect $S^+/S \leq C^+/C \leq He^0/He$; moreover to obtain the total He abundance we have assumed that $S^+/S = He^0/H$, therefore we will also assume that $S^+/S = C^+/C$.

Although the i_{cf} for C^+ and He^0 might be slightly higher than those used in Tables 15 and 17, we do not expect them to be much higher because the regions of low degree of ionization would yield higher He/H and C/H ratios than the regions with high degree of ionization.

V. DISCUSSION AND CONCLUSIONS

a) *Chemical Composition of M17, the Orion Nebula and the Sun*

In Table 18 we present the chemical composition of M17 for three values of t^2. The heavy elements by mass, Z, were derived under the following assumptions: a) CNO comprise 71% of the heavy elements abundance, by analogy with the solar abundances (see Table 19) and, b) in M17 20% of the O abundance is locked up in dust grains (Meyer 1985); this assumption is based on the idea that 15% of the O is locked in silicate cores and 5% in polymer mantles. The $\Delta Y/\Delta Z$ ratio was derived under the assumption that the primordial helium abundance by mass, Y_p, is equal to 0.230 (Torres-Peimbert, Peimbert, & Fierro 1989; Pagel *et al.* 1992).

For the Orion nebula we present in Table 19 the values for $t^2 = 0.00$ and 0.035 by Peimbert & Torres-Peimbert (1977) hereinafter PTP), the values for $t^2 = 0.00$ by Osterbrock *et al.* (1992) and the adopted values for $t^2 = 0.035$ from this article.

TABLE 18

CHEMICAL COMPOSITION FOR M17[a]

Element	$t^2 = 0.00$	$t^2 = 0.02$	$t^2 = 0.04$
He	11.02	11.01	11.00 ± 0.012
C	8.74	8.74	8.73 ± 0.05
N	7.71	7.86	8.01 ± 0.1
O	8.51	8.66	8.81 ± 0.06
Ne	7.80	7.96	8.13 ± 0.08
S	6.99	7.15	7.32 ± 0.1
Cl	5.18	5.33	5.48 ± 0.2
Ar	6.38	6.50	6.63 ± 0.1
Fe	6.62	6.78	6.94 ± 0.2
Y	0.291	0.286	0.280 ± 0.006
Z	0.0132	0.0161	0.0200 ± 0.003
$\Delta Y/\Delta Z$	4.47	3.48	2.50 ± 0.5

[a] Given in $12 + \log N(X)/N(H)$, with the exception of Y and Z that are given by mass.

TABLE 19

CHEMICAL COMPOSITION FOR THE SUN AND THE ORION NEBULA[a]

Element	Abundance				
	Sun	Orion Nebula			
t^2	...	0.00	0.00	0.035	0.035
He	10.99 ± 0.035	11.02	11.00	11.00	11.00
C	8.56 ± 0.04	8.55	8.57	8.52	8.53
N	8.00 ± 0.05	7.57	7.72	7.76	7.84
O	8.93 ± 0.035	8.52	8.49	8.75	8.74
Ne	8.09 ± 0.1	7.66	7.60	7.90	7.94
S	7.21 ± 0.06	7.19	6.97	7.41	7.19
Cl	5.5 ± 0.3	4.95	5.08	5.15	5.28
Ar	6.56 ± 0.1	6.6	6.41	6.7	6.51
Fe	7.67 ± 0.03	...	6.43	...	6.63
Y	0.275 ± 0.016	0.292	0.282	0.281	0.281
Z	0.0195 ± 0.002	0.0109	0.0111	0.0155	0.0155
$\Delta Y/\Delta Z$	2.33 ± 0.9	5.69	4.73	3.31	3.31
References[b]	1,2	3	4	3	5

[a] Given in 12 + log N(X)/N(H), with the exception of Y and Z that are given by mass.

[b] 1. Grevesse & Anders 1989; 2. Grevesse *et al.* 1990; 3. Peimbert & Torres-Peimbert 1977; 4. Osterbrock *et al.* 1992; 5. This paper.

The adopted values for $t^2 = 0.035$ were derived as follows: a) we recomputed the values by Osterbrock *et al.* for $t^2 = 0.035$, b) for He, C, N and O we took the average values between PTP and Osterbrock *et al.*, c) for Ne we used the value from PTP and the ionization correction factor from Mathis (1985), d) for S, Cl, Ar and Fe we used the values by Osterbrock *et al.* and, e) for Z and $\Delta Y/\Delta Z$ we adopted the M17 assumptions (see above).

The abundances by number for the Orion nebula and M17 correspond to the gaseous component, while the abundances by mass take into account the fraction of heavy elements embedded in dust.

Also in Table 19 we present the solar abundances from a compilation by Grevesse & Anders (1989), with the exception of N for which we used the result by Grevesse *et al.* (1990).

b) *The Value of* t^2

In Table 18 we present the abundances of the elements for three values of t^2, from this table it will be possible to derive abundances for other t^2 values. The He/H and C/H values are almost independent of t^2 but not those derived from a ratio of a collisionally excited line to a recombination line. The listed errors for $t^2 = 0.04$ include the errors on T and on the line intensities, but do not include the errors on t^2.

There is one observational result in favor of a large value of t^2 and it is given by the comparison of the Balmer and the [O III] temperatures; the error of this determination is very large and other arguments are needed to establish whether t^2 is different from 0.00 or not. From Figure 6 it is found that $| t^2 - \langle t^2 \rangle | \leq 0.005$ for all lines of sight, this result is easily explained for $t^2 \approx 0.01$; on the other hand if large values of t^2 are real ($t^2 \sim 0.04$), the inhomogeneous temperature structure has to be present along all lines of sigh and without significant variations from one line o sight to another, i.e., the mechanism producing the temperature inhomogeneities has to be present with similar strength along all lines of sight.

There are several observational determination of t^2 for the Orion nebula in the $0.011 < t^2 < 0.047$ range (e.g., Torres-Peimbert, Peimbert, & Daltabuit 1980 and references therein); all these determinations show very large errors but what is remarkable is that all of them yield positive values for t^2. Maybe the best way to determine t^2 is by comparing the C^{++} abundance derived from the $\lambda\lambda$1907, 1909 collisionally excited lines and tha

lerived from the λ4267 C^+ recombination line. A ecent application of this method yields $t^2 \sim 0.04$ or the Orion nebula (Walter 1991; Walter, Dufour, & Hester (1992).

From photoionization models of spherical nebulae Garnett (1992) has obtained that for T(O III) = 8200 °K, t^2(O III) = 0.006 while for T(N II) = 8700, t^2(N II) = 0.031. Gruenwald & Viegas (1992) have obtained for their A2O6 model (solar abundances, $N_e = 100\ cm^{-3}$ and spectral type O6) that t^2(O III) ~ 0.01 and t^2(N II) ~ 0.01 for different lines of sight. From both studies it follows that t^2 diminishes with an increase of T^* and T_e.

By fitting the observed [O II] and [O III] nebular lines with photoionization models of the Orion nebula it is found that the λ4363 [O III] auroral line is predicted to be fainter than observed (Simpson *et al.* 1986; Rubin *et al.* 1991; McGaugh 1991; Walter *et al.* 1992). The intensity of λ4363 could be reconciled with the models in the presence of additional sources of energy, like shock waves. Shock wave dissipation would increase the intensity of λ4363 leaving the nebular lines almost unaffected (Peimbert, Sarmiento, & Fierro 1991). To reconcile the observed and predicted λ4363 intensities, values in the $0.035 \leq t^2 \leq 0.058$ range are needed.

It is also possible to compare the M17 abundances with stellar abundances. It is expected in H II regions for C/O to be smaller than unity, which from the values in Table 18 implies that $t^2 > 0.02$ (assuming that O has to be increased by 0.08 dex in Table 18, to include the amount tied up in dust grains). Values of $t^2 \sim 0.04$ would be required to yield similar O/H and N/H ratios in M 17 and the sun (see Tables 18 and 19). Values of $t^2 \sim 0.02$ are needed to have similar O/H ratios in M17 and early B-type stars (Gies & Lambert 1992). Since M17 is ~ 2.1 kpc closer to the nucleus of the Galaxy than the sun and the early-B type stars studied by Gies & Lambert, and considering the presence of radial abundance gradients in the d(log X/H)/dR ≈ 0.06-0.10 kpc^{-1} range for C/H, O/H and N/H (see below), it would be necessary to increase the t^2 values to ~ 0.06 to reach agreement between the sun and M17 and to ~ 0.04 to reach agreement between the early-B type stars and M17.

Finally the Fe abundance is about one order of magnitude smaller in M17 than in the sun; which probably implies that most of the Fe in M17 is locked into dust grains. A similar result was obtained for the Orion nebula by Osterbrock *et al.* (1992).

More observational work on M17 is needed to determine an accurate t^2 value.

c) *C/H Galactic Abundance Gradient*

Chini, Elsässer, & Neckel (1980) find a photometric distance of 2.2 kpc for M 17, which combined with a distance of 450 pc to the Orion nebula (Sharpless 1952; Johnson & Hiltner 1956) imply a radial galactocentric difference between both objects of 2.5 ± 0.2 kpc. From the values in Tables 18 and 19 we derive a C abundance gradient of d(log C/H)/dR = −0.08 ± 0.02 kpc^{-1}, this result is independent of the t^2 value and is similar to the O gradients derived by other authors from H II regions and planetary nebulae (Peimbert 1978; Shaver *et al.* 1983; Faúndez-Abans & Maciel 1986).

This is the first time that the C/H gradient is derived in the literature. The C/H gradient might be very important in the determination of the CO to H_2 conversion factor as a function of galactocentric distance.

d) $\Delta Y/\Delta Z$

In Figure 18 we present the Y and Z values for Orion and M17 for $t^2 = 0.035$ and 0.04 respectively; in this figure we also present the Y and Z values for the SMC, the LMC, NGC 5471 and NGC 2363 for $t^2 = 0.00$ (Torres-Peimbert *et al.* 1989; Peimbert & Torres-Peimbert 1974, 1976; Dufour 1984; Dufour, Schiffer, & Shields 1984; Peimbert, Peña, & Torres-Peimbert 1986). The t^2 values for the last four objects might be different from zero but in general we expect smaller t^2 values for smaller Z values. Reviews on the $\Delta Y/\Delta Z$ determinations and theoretical predictions have been presented by Peimbert (1986) and Shields (1990).

We expect the $\Delta Y/\Delta Z$ ratio of M17 to be a

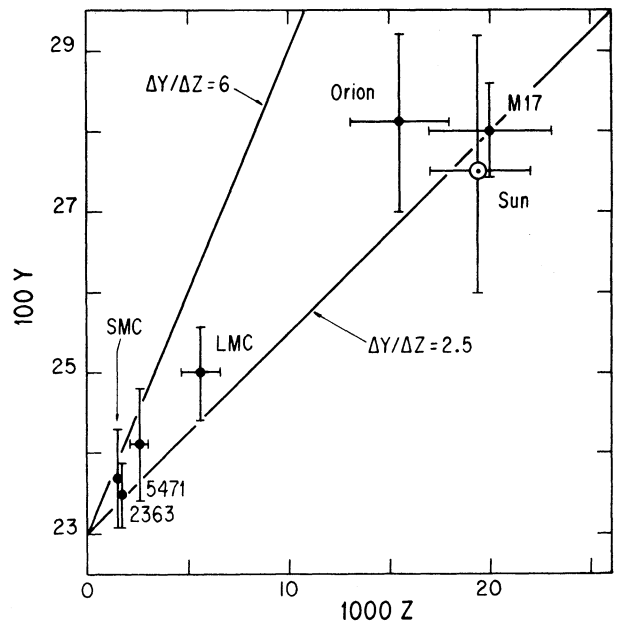

Fig. 18. Helium, Y, versus heavy elements abundance, Z, by mass. See text and Tables 18 and 19.

good observational constraint for stellar and galactic evolution models due to the high quality of the Y determination and to the large ΔY and Z baselines. In particular the accuracy in the Y determination is higher than for the Orion nebula due to the smaller contribution of neutral helium to the total He abundance.

From detailed photoionization models of the central regions of the Orion nebula Rubin *et al.* (1991) find that $He^0/He^+ = 0.20$ while Baldwin *et al.* (1991) find that $He^0/He^+ = 0.02$. Alternatively from optical observations PTP estimate that for the central regions $0.09 \leq He^0/He^+ \leq 0.16$ where the He^0/He^+ ratio increases with distance from the Trapezium, this increase has been confirmed by radio observations (Peimbert *et al.* 1988). In any case the uncertainty in the He/H ratio introduced by the presence of neutral helium in the Orion nebula makes its Y value more uncertain than that of M17.

Pagel *et al.* (1992) from observations of extragalactic H II regions find that $\Delta Y/\Delta Z$ is larger than 3 with a preferred value between 4 and 5. The results presented in Tables 18 and 19 are in good agreement with those derived by Pagel *et al.* and are considerably higher than the predictions from stellar evolution models. We note that the objects with WR features were not included in the $\Delta Y/\Delta Z$ determination by Pagel *et al.*; moreover these objects show higher Y values than objects without WR features and similar Z values, Pagel *et al.* have suggested that this result is due to contamination of the H II region material by winds of Wolf-Rayet stars (or their red supergiant progenitors). Alternatively we propose that the H II regions with WR features are affected by shock waves produced by the winds of the WR stars and consequently that they show larger t^2 values than the other objects, the effect would be to reduce Y and increase Z. A way to test this suggestion is to determine the widths of the emission lines in the H II regions; we would expect larger line widths for the objects with WR features than for the objects without them.

e) *Y versus C/H Diagram*

Based on the references for Figure 18 we present in Figure 19 the Y versus C/H diagram. In this diagram the Y and C/H values for Orion and M17 are almost independent of t^2 since the H, He and C abundances were derived from recombination lines; the other C abundances were derived from collisionally excited *UV* lines of C II and C III and are very sensitive to the t^2 value adopted. All the objects should lie along a straight line if all had the same: a) initial mass function, b) average age of the stellar component and, c) history of gas flows. The objects do not lie in a straight line. The distribution

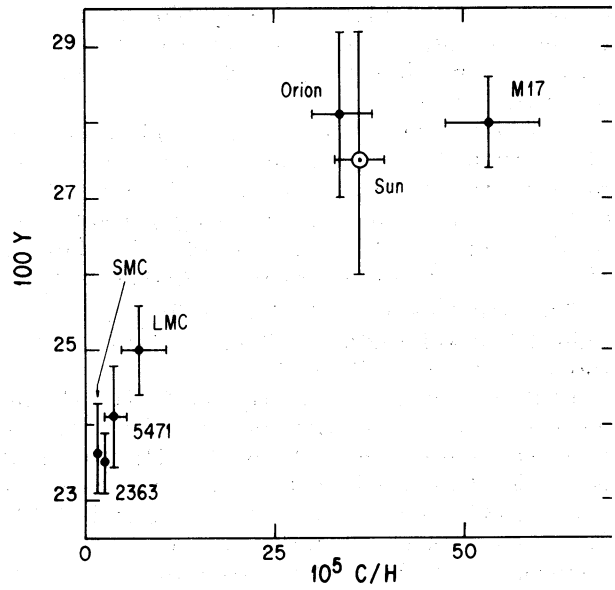

Fig. 19. Helium by mass versus $N(C)/N(H)$. See text and Tables 18 and 19.

is compatible with a delay of the C enrichment relative to the He enrichment. The delay could be due to the larger contribution of intermediate mass stars than that of massive stars to the C enrichment of the interstellar medium (e.g., Peimbert 1985 and references therein), while the He enrichment would have to be due to stars with a higher average mass. This delay would imply that the average age of the stellar content of a given system increases with C/H. A similar result is obtained from the C/O versus O/H diagram for galactic and extragalactic H II regions (Peimbert (1985). Another explanation for the distribution in Figure 19 is that the fraction of intermediate mass stars increases with Z.

It is a pleasure to acknowledge R.J. Dufour for a critical reading of the manuscript and for several excellent suggestions.

REFERENCES

Auer, L.H., & Mihalas, D. 1972, ApJS, 24, 193
Baker, J.G., & Menzel, D. H. 1938, ApJ, 88, 52
Baldwin, J.A., Ferland, G.J., Martin, P.G., Corbin, M.R. Cota, S.A., Peterson, B.M., & Slettebak, A. 1991, ApJ 374, 580
Brocklehurst, M. 1972, MNRAS, 157, 211
Chini, R. Elsässer, H., & Neckel, T. 1980 A&A, 91, 186
Churchwell, E., Smith, L.F., Mathis, J., Mezger, P.G., & Huchtmeier, W. 1978, A&A 70, 719
Clegg, R.E.S. 1987, MNRAS, 229, 31p
Conti, P.S. 1971, ApJ, 170, 325
_____. 1973, ApJ, 179, 161
_____. 1974, ApJ, 187, 539

Conti, P.S., & Alschuler, W. 1971, ApJ, 170, 325
Cox, D.P., & Daltabuit, E. 1971, ApJ, 167, 257
Dufour, R.J. 1984, in IAU Symposium 108, Structure and Evolution of the Magellanic Clouds, eds. S. van den Bergh and K.S. de Boer (Dordrecht:Reidel), p. 353
Dufour, R.J., Schiffer, F.H., III & Shields, G.A. 1984, in Future of Ultraviolet Astronomy Based on Six Years of IUE Research, ed. J.M. Mead et al. (NASA CP-2349), p. 111
Fañndez-Abans, M., & Maciel, W.J. 1986, A&A, 158, 228
Felli, M., Churchwell, E., & Massi, M. 1984, A&A, 136, 53
Ferland, G.J., & Cota, S.A. 1988, BAAS, 19, 1111
Garnett, D.R. 1992, AJ, 103, 1330
Gies, D.R., & Lambert, D.L. 1992, ApJ, 387, 673
Grevesse, N., & Anders, E. 1989, in Cosmic Abundances of Matter, ed. J. Waddington (New York: American Institute of Physics), p. 1
Grevesse, N. Lambert, D.L., Sauval, A.J., van Dishoeck, E.F., Farmer, C.B., & Norton, R.H. 1990, A&A, 232, 225
Gruenwald, R.B., & Viegas, S.M. 1992, ApJS, 78, 153
Hummer, D.G., & Storey, P.J. 1987, MNRAS, 224, 801
_____. 1992, NMRAS, 254, 277
Johnson, H.L., & Hiltner, W.A. 1956, ApJ, 123, 67
Kurucz, R.L. 1979, ApJS, 40, 1
Lester, D.F., Dinerstein, H.L., Rank, D.M., & Wooden, D.H. 1983, ApJ, 275, 130
Lichten, S.M., Rodríguez, L.F., & Chaisson, E.J. 1979, ApJ, 229, 524
Mathis, J.S. 1985, ApJ, 291, 247
Mathis, J.S., & Rosa, M.R. 1991, A&A, 245, 625
McGaugh, S.S. 1991, ApJ, 380, 140
McGee, R.X., & Newton, L.M. 1981, MNRAS, 196, 889
Mendoza, C. 1983, in IAU Symposium 103, Planetary Nebulae, ed. D.R. Flower (Dordrecht:Reidel), p. 143
Meyer, J.P. 1985, ApJS, 57, 173
Ogura, K., & Ishida, K. 1976, PAS Japan, 28, 35
Oke, J.B. 1974, ApJS, 27, 21
Osterbrock, D.E., Tran, H.D., & Veilleux, S. 1992, ApJ, 389, 305
Pagel, B.E.J., Simonson, E.A., Terlevich, R.J., & Edmunds, M.G. 1992, MNRAS, 255, 325
Peimbert, M. 1967, ApJ, 150, 825
_____. 1971, Bol. Obs. Tonantzintla y Tacubaya, 6, 29
_____. 1978, in IAU Symposium 76, Planetary Nebulae, ed. Y. Terzian (Dordrecht:Reidel) p. 215
_____. 1985, in Star Forming Dwarf Galaxies and Related Objects, eds. D. Kunth, T.X. Thuan, and J. Tran Thanh Van (Gif/Yvette: Editions Frontièrs), p. 403
_____. 1986, PASP, 98, 1057
Peimbert, M., & Costero, R. 1969, Bol. Obs. Tonantzintla y Tacubaya, 5, 3
Peimbert, M., Peña, M., & Torres-Peimbert, S. 1986, A&A, 158, 266
Peimbert, M., Rodríguez, L.F., Bania, T.M., Rood, R.T., & Wilson, T.L. 1992, ApJ, 395, 484
Peimbert, M., Sarmiento, A., & Fierro, J. 1991, PASP, 103, 815
Peimbert, M., & Torres-Peimbert, S. 1974, ApJ, 193, 327
_____. 1976, ApJ, 203, 581
_____. 1977, MNRAS, 179, 217
_____. 1987, RevMexAA, 14, 540
Peimbert, M., Ukita, N., Hasegawa, T., & Jugaku, J. 1988, PAS Japan, 40, 581
Pequignot, D. 1980, A&A, 81, 356
Robbins, R.R. 1968, ApJ, 151, 511
Robbins, R.R., & Bernat, A.P. 1973, Mém. Soc. R. Sci. Liege, 6th Ser., 5, 263
Rubin, R.H., Simpson, J.P., Haas, M.R., & Erickson, E.F. 1991, ApJ, 374, 564
Sánchez, L.J., & Peimbert, M. 1991, RevMexAA, 22, 285
Seaton, M.J. 1964, MNRAS, 127, 177
_____. 1978, in IAU Symposium 76, Planetary Nebulae, ed. Y. Terzian (Dordrecht:Reidel), p. 131
Sharpless, S. 1952, ApJ, 116, 251
Shaver, P.A., McGee, R.X., Newton, L.M., Danks, A.C., & Pottasch, S.R. 1983, MNRAS, 204, 53
Shields, G.A. 1990, ARA&A, 28. 525
Simpson, J.P., Rubin, R.H., Erickson, E.F., & Haas, M.R. 1986, ApJ, 311, 895
Smits, D.P. 1991, MNRAS, 248, 193
Stone, R.P.S. 1977, ApJ, 218, 767
Stone, R.P.S., & Baldwin, J.A. 1983, MNRAS, 204, 347
Torres-Peimbert, S., Peimbert, M., & Daltabuit, E. 1980, ApJ, 238, 133
Torres-Peimbert, S., Peimbert, M., and Fierro, J. 1989, ApJ, 345, 186
Vílchez, J.M., & Pagel, B.E.J. 1988, MNRAS, 231, 257
Walter, D.K. 1991, PASP, 103, 830
Walter, D.K., Dufour, R.J., & Hester, J.J. 1992, ApJ, in press
Whitford, A.E. 1958, AJ, 63, 201

Manuel Peimbert and Silvia Torres-Peimbert: Instituto de Astronomía, UNAM, Apartado Postal 70-264, 04510 México, D.F., México.
María Teresa Ruiz: Depto. de Astronomía, Universidad de Chile, Casilla 36-D, Santiago, Chile.